Drew University
College of Liberal Arts

Investigation of Stereochemical Structural Changes to Inhibit the Human *In Vitro* Metabolic Rate of Chemical Mutant p53 Reactivators as a Potential Oncology Therapy

An Honors Thesis in Biochemistry and Molecular Biology
By
Danielle D. Millick

Submitted in partial fulfillment
Of the Requirements
For the degree of
Bachelor in Arts
With Specialized Honors in Biochemistry and Molecular Biology

April 2017

ABSTRACT

Even if a drug candidate has high biological activity, selectivity and decent drug-like properties, without a reasonable metabolic rate, it will not have much success. Previously quinolone and benzimidazole class compounds have been synthesized and shown to reactivate mutated forms of the transcription factor protein, p53, which is a reoccurring mutation motif in cancer cells. Additionally a metabolism assay has been designed and employed using human liver microsomes, containing Cytochrome P450 enzymes, and the cofactor NADPH in order to determine human clearance and half-life of these compounds. Previous findings in this study indicate that the presence of an electron-withdrawing group on the side of the benzimidazole derivatives where metabolism is taking place, inhibited metabolism and produced a larger *in vitro* human half-life (in minutes). The aim of the current study was to determine whether not only the electronegativity but also the size of the electron-withdrawing group being added (F, Cl, Br, and I) had an effect on the metabolic rate. The concentration of our parent compound and metabolites were monitored via quantitative liquid chromatography mass spectrometry, throughout the duration of the assay. This approach allowed us to establish metabolic profiles for our benzamidazole derivatives, and make structural modifications in order to achieve *in vitro* human clearance rates similar to those of marketed drugs Midazolam: $t_{1/2}$ = 49.6 min., and Propranolol: $t_{1/2}$ = 20.5 min. In this study, Chloro-, Bromo-, and Iodo- compounds demonstrated smaller half-lives (68.6/19.3 min, 25.2 min,

and <<15 min, respectively) compared to the Fluoro- compound (half-life of 30 min). We found that electronegativity of the substituent added had a greater effect on the inhibition of metabolism versus the size of the substituent, when added at that indicated position of the ring.

TABLE OF CONTENTS

Section **Page**

GLOSSARY……..……..

INTRODUCTION……..…… 1

The Drug Discovery Process……...…… 1

Potency and Selectivity……...……2

Membrane Transport……....……....……3

Drug Metabolism and Pharmacokinetics……..……..……..4

Cytochrome P450 and Drug Metabolism..…….……5

Enhancing Metabolic Stability……....……... ……11

In vitro Prediction of Metabolic Rate…..…… ……...15

Inhibition of CYP450……..……...……..16

Cancer and Clinical Significance……..……..…… 18

Role of p53 in Cancer.……..……..……..…..19

MDM2/MDM4 Inhibition of Wildtype p53……..……..…..23

p53 Reactivation……..……...24

RESEARCH OBJECTIVE…….……...26

EXPERIMENTAL……..……29

Background……..……....29

Liquid Chromatography-Mass Spectrometery…….....29

Nuclear Magnetic Resonance Spectroscopy……..……..……31

Synthetic Strategy.……..……33

Reagents……..……..……37

Characterization……..37

Synthetic Pathways……..38

Synthesis of Intermediates……..…….....38

Chloro-Intermediate……..……38

Bromo-Intermediate……..……40

Iodo-Intermediate……..……43

Synthesis of Final Products……46

Chloro-urea (RD 88) ……..…..46

Bromo-urea (RD 97) ……..……...……..49

Iodo-urea (RD 98) ……..……..……..52

Phase I In vitro *Metabolism*……....55

Solutions……..…55

Procedure……56

Compound Concentration Calculation……...56

Identification of Metabolites……..……..57

Metabolic Rate Calculations……...……59

RESULTS…….……..……61

DISCUSSION…….……..……..68

Characterization Data…….68

Metabolism Assays……..…….69

RD 88……..…….69

RD 97……70
RD 98……70
Conclusions……73
Future Considerations……76
REFERENCES..……78

GLOSSARY

ADME: absorption distribution metabolism excretion of a compound
Angiogenesis: development of new blood vessels
Apoptosis: process of programmed cell death
BAX: BCL2-associated X protein involved in apoptosis
Blood Brain Barrier (BBB): Highly-selective permeable membrane separating brain from circulatory system
Cancer: group of diseases involving abnormal cell growth and invasion into other tissues
Carcinogenicity: any substance that is directly involved with causing cancer
Cell: basic structural, functional, and biological unit of living organisms
Chromatogram: a visible record showing the results of separation of the components of a mixture by chromatography
Clearance: pharmacokinetic measurement of the volume of plasma that is completely cleared off of a substance per unit of time
Cofactor: a compound or metallic ion that is essential for the activity of an enzyme
CYP450: Family of enzymes that are located in the liver and are responsible for drug metabolism
DMPK: Drug Metabolism Pharmacokinetics
GI: gastrointestinal tract
HPLC: High Performance Liquid Chromatography
Isozymes: enzymes that serve the same function (catalyze the same reaction) but differ in structure
LC/MS: Liquid Chromatography-Mass Spectrometry
Lipophilicity: the ability of compound to dissolve in a non-polar solvent (such as oil or hexane)
NMR: Nuclear Magnetic Resonance Spectroscopy
Pharmacokinetics (PK): the time course of compound and metabolite concentrations in the body which includes absorption, distribution, metabolism and excretion.

INTRODUCTION

The Drug Discovery Process

The drug discovery process involves the development and optimization of chemical compounds that target a specific element of a given pathology, in order to eventually produce marketable drugs for the safe and effective treatment of the disease. Once lead structures, or "hits" are identified, through methods such as Chemical Library screening or High Throughput Screening (HPTS), and target validation is confirmed, these lead compounds are modified to improve potency, selectivity and drug-like properties, including human metabolic stability and membrane permeability (Mizuno *et al.* 2003).

However early on in the history of drug discovery, finding active compounds was the primary focus, and factors such as pharmacokinetics (PK), toxicity, solubility, and stability were not considered until later in the development stage (Kerns and Di 2011). Due to the high cost and low yield that was associated with this method, it became clear early intervention would be necessary, and this screening process was enhanced in order to determine if compounds had acceptable PK, toxicity, and stability before advancing in the development process. These compounds with a favorable profile of potency, selectivity and drug-like properties are further evaluated to determine *in vivo* bioavailability, efficacy and toxicity. Once an optimized candidate compound is identified, progression to toxicology studies and clinical trials in humans can begin. A summary of the major steps which comprise this process is provided in **Table 1** (Mizuno

et al. 2003). Eventually a successful outcome of efficacy versus toxicity can lead to a marketed drug, and these properties are contingent upon a drug's potency and selectivity.

Table 1: Outline of Drug Discovery Process	
1.	Identification, validation, and development of assays for the biological target relevant to a disease state.
2.	Screening and identification of lead structures.
3.	Optimization of lead structures to increase potency and selectivity.
4.	Optimization of lead structures to improve *in vitro* drug-like properties.
5.	*In vivo* studies to evaluate efficacy and toxicity.
6.	Clinical trials in humans with most promising compounds.

Potency and Selectivity

Potency in terms of pharmacology is a measure of drug activity describing the amount of drug or compound required to produce a response of necessary intensity (Kerns and Di 2011). Additionally potency directly relates to required administration method. For example if a compound has average or low potency it would require intra-venous (IV) administration so the drug could be administered directly to the circulatory system and not have to face any barriers that could possibly lower the amount of drug that reaches the circulatory system. However if a drug has high potency or activity, then all administration routes are available and the optimal administration route can be decided on other parameters.

In drug discovery, the term selectivity refers to the compound or drug being selective towards the desired target. If a compound is not selective, this means that it could bind to important components of the cell (other than the target, such as ion channels and various receptors) and alter their functions, which could result lower levels or target-activity and even in off-target cytotoxicity. In the drug development process selectivity screens are typically performed on promising advanced lead compounds against a variety of cellular targets (Kerns and Di 2011).

Membrane Transport

Membrane transport or membrane permeability refers to compound or drug's ability to cross biological membranes within the body, such as the gastrointestinal (GI) membrane or the blood-brain-barrier (BBB). Drug permeation of these membranes can occur through several different mechanisms, such as passive diffusion, endocytosis, uptake transport (through a transporter), and paracellular transport (through cell junctions) (Kerns and Di 2011). Compound ability to cross biological membranes is important because it can determine other parameters such as bioavailability and administration method. For instance, GI membrane permeability is required for a drug to be administered orally, and while the BBB is a very selective membrane (estimated that only 2% of the possible CNS compounds cross), its permeability is required if the biological target is within the brain (Kerns and Di 2011). Another parameter that must be considered in membrane transport is efflux or the active transport of compound from the intracellular space back into the lumenal space (Kerns and Di 2011). This property serves

several functions depending on the biological membrane, for example efflux is primarily carried out by P-glycoprotein in the BBB and serves a protective function by removing foreign molecules before they reach brain tissues.

Drug Metabolism and Pharmacokinetics

Drug metabolism and pharmacokinetics (DMPK) are two other areas of consideration in drug discovery. Pharmacokinetics (PK) is the study of the time course of compound and metabolite concentrations in the body (Kerns and Di 2011). Pharmacokinetics describes the process of Absorption, Distribution, Metabolism, and Excretion (ADME) of a compound when administered to a living animal (Nichols *et al.* 2007). The absorption of a drug can be predicted by its transport rate across biological membranes in the GI track. After crossing the intestinal GI membranes, the compound enters the portal vein and goes directly to the liver, where first-pass metabolism takes place (Ruiz-Garcia *et al.* 2008). The remaining compound and metabolites then enter the general circulatory system where drug distribution occurs to various tissues throughout the body (Ruiz-Garcia *et al.* 2008). Parent drug and metabolites can have different biological effects. The compounds in the circulatory system eventually reenter the liver for additional metabolism then all metabolites and un-metabolized parent drugs are excreted, or cleared from the circulatory system. The longer that the drug or parent compound is present in the circulatory, the longer biological effect or activity will persist. The purpose of drug metabolism is to increase the polarity, or water solubility, of the

drug so that the metabolites can be excreted by the kidney or through the bile more easily.

Some more specific PK parameters of a compound that describe the drug metabolism aspect of ADME include half-life and clearance, which are determined by physiochemical and biochemical properties of the compound. These properties result from the chemical structure of the compound and how it is affected by the environment that it is administered into, and human *in vitro* half-lives ($t_{1/2}$) typically fall within the range of 25-50 minutes for most marketed drugs (Kerns and Di 2011). Initially the concentration of the parent compound in the circulatory system is high, and then it decreases as it is distributed to the tissues and drug metabolism occurs. Conversely, first pass metabolism forms a small amount of initial metabolite, which increases overtime, along with metabolite species becoming increasingly more polar until they are successfully excreted through the kidneys or the bile.

Cytochrome P450 and Drug Metabolism

Drug metabolism predominately occurs in the liver, and is primarily catalyzed by cytochrome P450 enzymes (CYP450s) (Huang *et al.* 2010, Nassar *et al.* 2004). CYP450s are a superfamily of proteins that contain a heme as a cofactor in order to catalyze enzymatic reactions for a multitude of substrates. They are typically terminal oxidase enzymes in electron transfer chains, and therefore broadly categorized as P450-containing systems since most CYPs require a both protein partner to deliver elections allowing for reduction of the iron (at the center of the heme) and molecular oxygen. This

family of enzymes is responsible for approximately 75% of drug metabolism with the CYP3A4/5, CYP2C9, CYP2C19, CYP2D6, and CYP1A2 isozymes metabolizing the majority of marketed drugs (Guengerich 2008) (**Figure 1**).

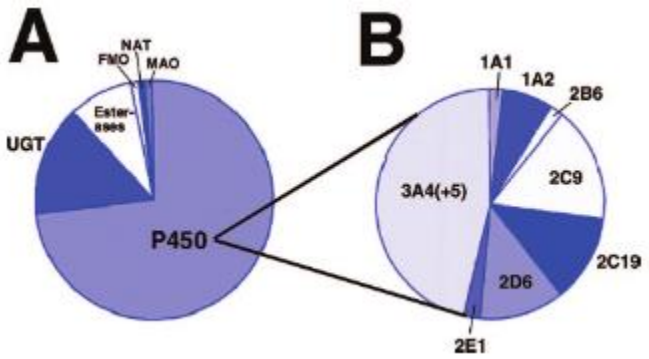

Figure 1. Breakdown of enzymes responsible for metabolism of marketed drugs **A.** CYP450 (P450) family of enzymes is responsible for ~75% of metabolism of 57 marketed drugs. Glucuronosyltransferase (UGT), esterases, flavin-containing monooxygenase (FMO), N-acetyltransferase (NAT), and L-Monoamine oxidases (MAO) are the other enzymes represented with their indicated contributions towards drug metabolism. **B.** Breakdown of individual CYP450 isozymes and their contributions to the metabolism of these drugs. CYP3A4/5, CYP2C9, CYP2C19, CYP2D6, and CYP1A2 are responsible for the metabolism of most of the drugs evaluated in this study by Pfizer. Researchers noted that similar percentages were reported by other pharmaceutical companies (Figure from Guengerich 2008).

The most common reaction catalyzed by CYP450 enzymes is a monooxygenase reaction, which is the insertion of one atom of oxygen into the aliphatic position of an organic substrate (RH) forming a hydroxylated product (ROH) (Dorokhov *et al.* 2017) (**Figure 2**). This enzymatic reaction is the basis for phase I drug metabolism and allows the conversion of lipid soluble drugs into metabolites that are more water-soluble and therefore more easily excreted through the kidneys (renal excretion) (Seger *et al.* 2015).

The metabolites produced from phase I metabolism are known to be active in biological systems and may even have effects dissimilar to the parent compound, such as toxicity and carcinogenicity. In phase II metabolism, the hydroxyl becomes functionalized, or a larger polar group is added, in order to further enhance the polarity and excretion.

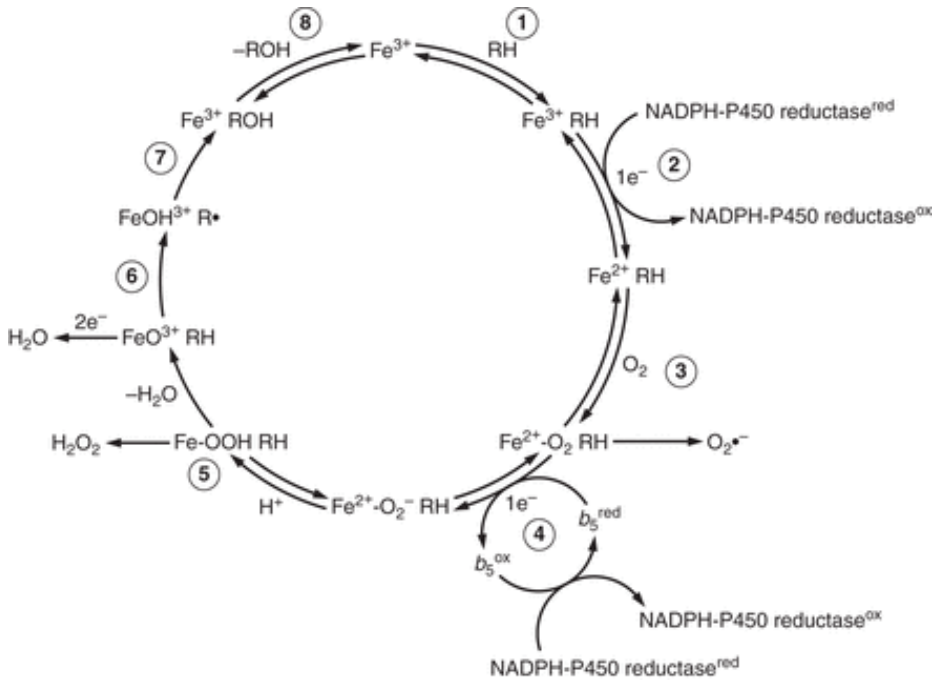

Figure 2. Mechanism of Phase I metabolism by CYP450
This is the general scheme for P450-catalyzed oxidation reactions of substrate or compound R-H. Following substrate binding (step 1), ferric P450 receives one electron via NADPH-P450 reductase (step 2). The ferrous form of heme binds oxygen (O_2) (step 3) before undergoing a second one-electron reduction to begin O_2 activation (step 4). Although this second electron originates from NADPH-P450 reductase, the accessory protein cytochrome b5 takes part in the delivery of the electron to P450. Insertion of the activated oxygen into the substrate occurs via C-H bond cleavage (step 6) followed by rapid oxygen rebinding to form the product (step 7). Finally the product, R-OH (metabolite) is released from the active site of the enzyme (Step 8) (Figure from Dorokhov *et al.* 2017).

Phase I metabolism is the rate-determining step, and thus it is commonly used to study the rate at which a drug is metabolized, *in vivo* and *in vitro* (Kerns and Di 2011). Two terms that are commonly used to describe this rate are half-life (the time it takes for a drug to reach half its initial concentration in the circulatory system) and intrinsic clearance (a measure of the liver's ability to remove drug from the body or circulatory system) (Kerns and Di 2011). Thus, improve metabolic stability of a compound can be indicated by an increased half-life and a decreased intrinsic clearance, allowing for the drug to be biologically active for a longer period of time.

However in order to successfully modulate the rate of drug metabolism an understanding of the responsible enzyme's specificity is required. Some insights into the varied binding specificities of the different CYP450 isozymes towards various functional groups, may provide useful information about which isozymes may have stronger affinities towards our compounds. For instance, one study examined binding interactions between various flavonoids, differing in terms of chain length, and CYP450 isozymes and determined that both steric contacts (resulting from changes in sugar chain length) and interactions from specific amino acid residues affected the interaction between the flavonoid and CYP450 isozyme (Sousa *et al.* 2017). Specifically, they found that certain key features contributed to the orientation of the flavonoid in the catalytic site such as the presence of a sugar chain on certain rings of the flavonoid and the polar and steric interactions of sugar chain towards these different rings of the flavonoids. Additionally they determined key residues of the 1A2 (Asp313, Phe226, Phe256 and Phe260) and 2C9 (Asn474, Ser209, Thr304 and Arg108) isozymes (two isozymes with highest rates of

metabolism for flavonoids evaluated) that were crucial for the regioselectivity and positioning of the substrate (Sousa *et al.* 2017). These findings indicate that steric contacts of a substrate may have a significant degree of influence on its CYP450 isozyme binding. While this study examines large structural changes such as chain length and their effects on enzyme binding, the impact of smaller structural changes such as changes in halogen size has not been investigated.

In another study, following the National Institutes of Health Chemical Genomics Center (NCGC) screening of a collection of over 17,000 compounds against the five major isozymes of CYP450 (1A2, 2C9, 2C19, 2D6, and 3A4) in a quantitative high throughput screening (qHTS) format, researchers developed support vector classification (SVC) models for these five isozymes using a set of customized generic atom types (Sun *et al.* 2017). Using this system they confirmed specificities of the CYP450 isozymes from different atoms and functional groups while. Some specific findings were that 3A4 typically bound molecules of high molecular weights (400-600 amu and >600 amu) and molecules with more aromatic rings (>3) while the 2D6 isozyme preferred substrates with less polar surface area (PSA between 0-20 angstroms^2) (Sun *et al.* 2011). Additionally the authors note the utility of these models towards prioritizing compounds in a drug discovery pipeline and recognizing toxicity potential of environmental chemicals towards CYP450 isozymes.

Another chemical property that can impact which CYP450 isozyme metabolizes a drug is lipophilicity. Lipophilicity describes the ability of a drug or compound to dissolve

$$LogP_{\left(\frac{octanol}{water}\right)} = \log\left(\frac{(compound)_{octanol}}{(compound)_{water}}\right) \qquad (1)$$

in a non-polar or hydro-phobic solvent, including lipids, oil, and hexane, and is typically measured by LogP which is the partition coefficient of a molecule between an aqueous and lipophilic solvents (typically octanol and water) described in equation (1).

One study investigated this idea by profiling a variety of marketed drugs against the isozymes responsible for their metabolism and were able to determine a range of lipophilicity (indicated by logP of the substrate/drug) that each CYP450 isozyme would accept based on the drugs that were metabolized by that isozyme (Lewis *et al.* 2004). This study indicated that only certain isozymes (CYP450 1A1, 1B1 and 3A4) displayed selectivity for compounds of higher lipophilicity (**Table 2**). These insights into enzyme affinity can potentially aid drug optimization efforts in terms of metabolic stability.

Table 2. CYP450 Isozyme Selectivity based on log P values

Table 3. Ranges and average log P values for human P450 substrates of families CYP1, CYP2 and CYP3

% Drugs[†]	CYP	Range of log P values	Average log P value (n)	Other characteristics	Typical substrate and log P
3	1A1*	1.39 to 6.35	3.41 [16]	Planar PAHs and their diols	DMBA-3,4-diol 3.42
10	1A2	0.08 to 3.61	2.01 [18]	Planar amines and amides	MeIQ 1.98
1	1B1	1.40 to 6.35	3.73 [12]	Planar PAHs and their diols	BP-7,8-diol 3.87[c]
3	2A6	0.07 to 2.79	1.44 [18]	Fairly small molecules	Losigamone 1.46
4	2 B6	0.23 to 4.89	2.54 [16]	Basic (Unionized)	Buproprion 2.54
	2C8	0.06 to 6.98	3.38 [12]	Acidic (Ionized)	Rosiglitazone 3.20
25	2C9	0.89 to 5.18	3.20 [18]	Acidic (Unionized)	Naproxen 3.18
	2C19	1.49 to 4.42	2.56 [16]	Amides and amines	Proguanil 2.53
15	2D6	0.75 to 5.04	3.08 [16]	Basic (Ionized)	Propranolol 3.09
3	2E1	-1.35 to 3.63	2.07 [20]	Small molecules	4-Nitrophenol 2.04
N/A	–2F1*	0.37 to 5.14	2.63 [12]	Fairly small molecules	3-Methylindole 2.72[c]
36	3A4	0.97 to 7.54	3.10 [50]	Large molecules	Nifedipine 3.17

Notes: Summary data from study indicates that log P value of a drug can provide insight into predicting which isozyme will carry out its metabolism (Table from Lewis *et al.* 2004).

Enhancing Metabolic Stability

Slight structural modifications to compounds can greatly improve their metabolic stability without causing large changes in activity. Several strategies to enhance metabolic stability that have been described in the literature which include: deactivation of aromatic rings with strongly electron-withdrawing groups, reducing the compound's lipophilicity, and removing or blocking labile groups (Nassar *et al.* 2004). One specific modification that is frequently used to slow a compound's metabolic rate (increase half-life) is the addition of fluorine atom, which blocks metabolism due to its high electronegativity (Kerns and Di 2011). This observed inhibition of metabolism is due to the electron-withdrawing property of the fluorine substituent which slows the free-radical hydroxylation by CYP450, however, this modification is sometimes undesirable due to fact that fluorine atoms can be biologically active independently (Kerns and Di 2011). In one specific example, a novel inhibitor of intestinal cholesterol absorption was biologically active but displayed poor PK properties. Using information obtained from QSAR (quantitative structure–activity relationship) metabolite studies developers added fluorine (inhibits metabolism due to electron-withdrawing property) and hydroxyl (blocks metabolism here by "pre-forming" metabolite) groups in labile areas to block metabolism at these sites and thus improve the oral PK by 50-fold (**Figure 3**) (Rosenblum *et al.* 1998).

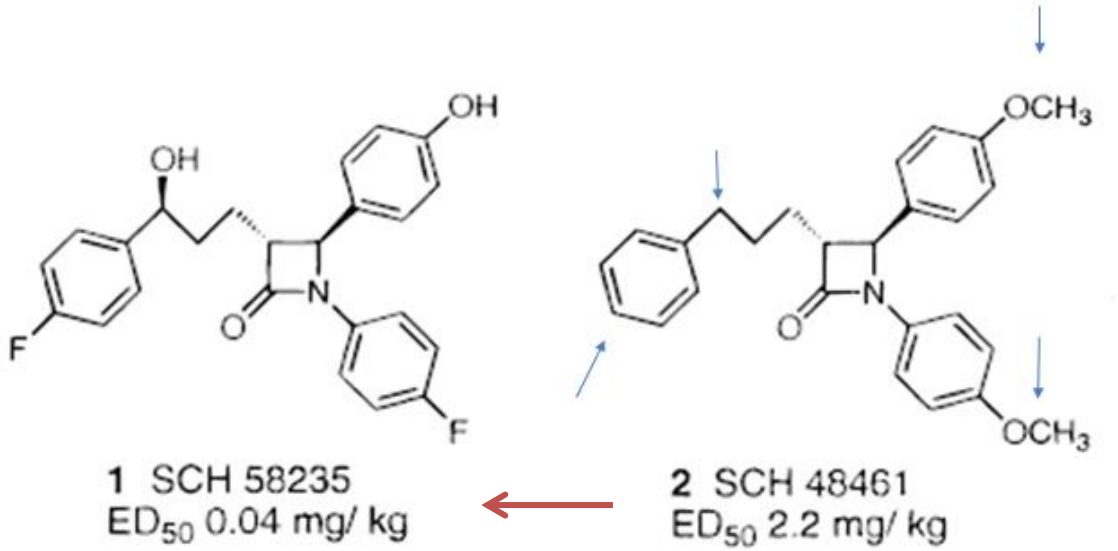

Figure 3. Enhanced metabolic stability of intestinal cholesterol absorption inhibitor Lead structure ((3R)-(3-Phenylpropyl)-1,(4S)-bis(4-methoxyphenyl)-2-azetidinone) (**2**) showed poor PK properties due to rapid phase I metabolism at depicted sites (arrows) (via hydroxylation or de-methylation), and was optimized by structural modifications (addition of fluorine and hydroxyl groups) at labile sites in order to improve oral PK by 50-fold. Market drug, *Zetia*, is depicted on the left (1, 1-(4-fluorophenyl)-(3R)-[3-(4-fluorophenyl)-(3S)-hydroxypropyl]-(4S)-(4-hydroxyphenyl)-2-azetidinone) (**1**). Adapted from Rosenblum *et al.* 1998.

Another example of how structural modification can improve PK is that researchers were able to improve the C_{max} (maximum serum concentration of drug in a target area following administration) of orally administered vinylacetylene antivirals by allylic oxidation of a labile site. And by introducing a second modification of phenyl oxidation (addition of a fluorine substituent) at another labile site they were able to increase the percent bioavailability (from 9.00 %F to 23.00 %F) of the compound

(inversely related to metabolic rate) with virtually no effect on the activity (IC_{50}) *in vivo* (**Figure 4**) (Nassar *et al.* 2004).

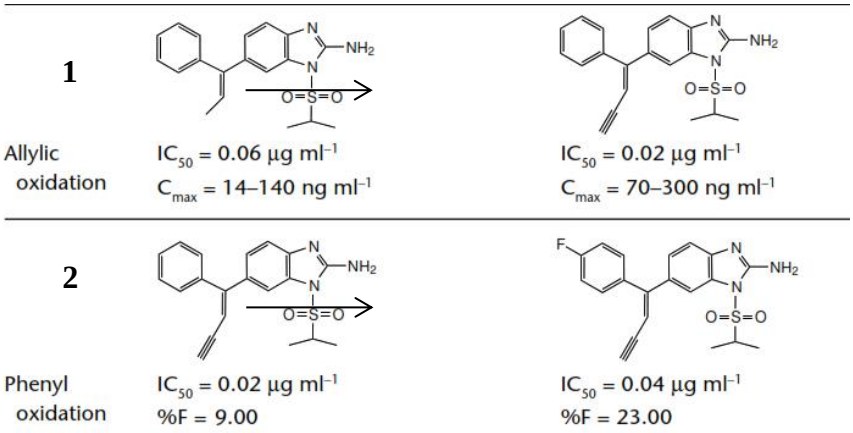

Figure 4. Enhanced PK of Vinylacetylene antivirals via stepwise structural modification
Allylic oxidation (via addition of triple bond) at labile site improved C_{max} (**1**). Then phenyl oxidation (via addition of flourine) improved % F (**2**). Structural modifications hardly impacted IC_{50} value. Adapted from Nassar *et al.* 2004.

Another structural modification strategy commonly used to block metabolism at labile sites is the addition of an oxetane (see **Figure 5-2**). While addition of a *gem*-dimethyl group (see **Figure 5-1**) has been commonly used to block metabolism at a labile site, when performed on small molecules this structural modification typically causes a large increase in lipophilicity which can in turn result in reduced metabolic stability and poor PK properties (Wuitschik *et al.* 2006). However by introducing a stable molecule that is similar in size and less metabolically active (such as oxetane) as an alternative blocking group at a labile site, metabolism of the compound can be inhibited without causing major effects on other PK parameters. This strategy was shown to be successful

as researchers were able to improve human (and mouse) in vitro $Cl_{int.}$ of N,N-dimethyl-4-(p-tert-butylphenyl)butylamine by adding oxetane functional groups to various positions (Wuitschik *et al.* 2006).

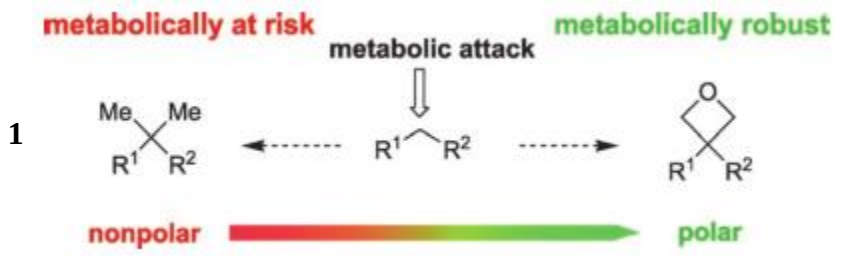

Figure 5. Oxetanes vs. gem-dimethyls as metabolism blocking groups
Gem-dimethyls (**1**) have been commonly used to block metabolism at labile sites, however this modification results in increased lipophilicity and thus poor PK. While oxetanes (**2**) are similar to gem-dimethyls in volume, they are more metabolically stable and therefore a better alternative. Adapted from Wuitschik *et al.* 2006.

Other structural modification strategies that are commonly used to block phase I metabolism include: altering ring size (large change in sterics), changing the chirality of a molecule, and removing or replacing unstable groups (Kerns and Di 2011). These improvements in metabolic stability and bioavailability are imperative for a drug to be successful, since improved metabolic stability results in lower doses and less frequent dosing. These less tedious drug regimens will be more desirable for patients and also easier to follow, and will therefore lead to improved patient compliance and ultimately more successful treatment. These properties of lead compounds can be evaluated using either *in vitro* or *in vivo* techniques during the drug development process to provide valuable insights for optimizing drug candidates.

In Vivo Metabolism Prediction via *In Vitro* Analysis

In order to evaluate the metabolic stability of compounds in an efficient and cost-effective way, *in vitro* techniques have been derived in order to predict human *in vivo* metabolism. Since organisms like mice conduct metabolism differently than humans and have different liver enzymes, *in vivo* animal models are not acceptable methods of predicting human metabolism (Kerns and Di 2011). One common approach of determining *in vitro* half-life and intrinsic clearance is by performing incubations with compound using human liver microsomes (purified liver fractions which contain cellular proteins and enzymes), NADPH (cofactor for metabolizing enzymes) and a physiological buffer **(**Obach 1999, Huang *et al.* 2010, and Chiba *et al.* 2009). By collecting aliquots at different time points and measuring the concentration of compound via quantitative LC/MS (liquid chromatography-mass spectrometry), half-life and intrinsic clearance can be calculated. This method was utilized in one study to evaluate numerous marketed drugs (Obach 1999) and has been validated as an effective method of predicting human drug metabolism *in vitro*.

The human liver microsomal approach is commonly used to evaluate metabolic stability of compounds in drug discovery process because the material contains a major portion of the metabolizing enzymes from a living system but can also be conducted in a high-throughput and relatively inexpensive manner (Kerns and Di 2011). However this system also has some limitations. For instance this approach only evaluates phase I metabolism, in addition it has been noted that drugs can non-specifically bind to human

liver microsomes depending on their physiochemical properties (McLure *et al.* 2000). In this study researchers found that three of the drugs (weak bases amiodarone, amitriptyline and nortriptyline) all bound extensively to the microsomal membrane, and that the binding was saturable for two of these drugs (nortriptyline (K_D~147 mM) and amitriptyline (K_D~178 mM) at 1 mg/mL) (McLure *et al.* 2000). These findings suggest that compounds of certain physiochemical characteristics (lipophilic weak bases) can integrate into the microsomal membrane and this binding could conceivably result in inaccurate data produced by this assay. There are other approaches of evaluating metabolic stability that do not contain these same limitations, such as using S9 (material containing broader set of metabolizing enzymes), hepatocytes (whole liver cells) or liver slices (conduct both phase I & II metabolism), however all approaches have tradeoffs that must be considered.

Inhibition of CYP450

While several CYP450 isozymes (enzymes that serve the same function but differ in structure) exist in the human liver and conduct drug metabolism, some drugs may be metabolized by the same isozyme, which could result in harmful drug-drug interactions (Kerns and Di 2011). Because of this it is helpful to determine which specific isozyme metabolizes a given drug or compound. This can be done by use of enzyme inhibitors, specifically CYP450 inhibitors. Many CYP450 inhibitors have been developed and are well classified in terms of which isozyme they specifically inhibit (**Table 3**) and new CYP450 inhibitors are being synthesized to this day due to their utility and relevance

(Sridhar *et al.* 2012, Fasinu *et al.* 2016). In addition, some natural compounds are known to be potent CYP450 isozymes inhbitors. For instance, one study noted that co-administration of calcium channel agonists with grapefruit juice can significantly increase bioavailability of the drug as a result of CYP3A4 inhibition, and these effects can even last up to 3 days (Hayashibara 2009). This isozyme inhibition can be harmful because increasing the bioavailability allows a drug to persist longer in the body, which could allow the drug to reach a harmful concentration and result in off-target toxicity. Because of this, physicians typically advise patients to avoid grapefruit juice when prescribing certain drugs (that are known to be metabolized by CYP3A4). Additionally if a patient is taking two drugs that are metabolized by the same CYP450 isozyme, then the drug that the isozyme has a lower affinity for will be metabolized at a slower rate (than it would be if taken alone, assuming that its metabolism is not inhibited entirely) which will also result in this drug having a potentially dangerous bioavailability. For these reasons it is important to know which CYP450 isozyme is responsible for the metabolism of a given drug in order to be able to predict and prevent drug-drug interactions (isozyme inhibition) and avoid harmful outcomes for patients that can be easily prevented with this information.

Table 3. CYP450 Isozymes and their respective known inhibitors

Isozyme	Inhibitor(s)
CYP 1A2	Cimetidine, Amiodarone, Ticlopidine
CYP 2C19	Cimetidine, Ketoconazole, Omeprazole
CYP2C9	Fluvastatin, Lovastatin, Isoniazid
CYP 2D6	Cimetidine, Fluoxetine, Methadone
CYP 2E1	Disulfiram, Water Cress
CYP 3A4,5,7	Cimetidine, Iarithromycin, Ketocnazole

Cancer and Clinical Significance

Cancer is characterized as a group of diseases in which abnormal cells divide without control and invade other tissues; in addition these cells can spread to other parts of the body through the circulatory and lymphatic systems (CDC 2017). A variety of factors (exposure to chemicals such as tobacco smoke, UV light and even viruses) can lead to cancer manifestation. These factors in addition to displayed variety in site of damage and tumor phenotype enhance the diversity of the disease and its potential impact on the human population. Cancer is the second leading cause of death in the United States and is only exceeded by heart disease (CDC 2017). Over 500,000 deaths per year in the United States are attributed to the disease, which translates to one of every four deaths being due to cancer. As the risk of developing any form of cancer is projected to increase,

it is imperative that researchers develop more effective therapeutic strategies for combating the disease.

Role of p53 in Cancer

One particular protein with evident relevance in cancer, and thus is the biological target of a substantial amount of all cancer research, is the transcription factor p53. As a tumor suppressor p53 is a transcription factor responsible for the regulation of many genes involved in cell regulation processes, such as apoptosis and DNA repair (Bullock and Fersht 2010). When p53 is activated through phosphorylation, it binds to DNA in a tetramer complex and activates the transcription of many cell control proteins. Different types of cellular stress, such ultra-violet (UV) light or DNA breaks, can lead to p53 activation, through ATM or ATR kinases, which results the transcription and expression of cell cycle control proteins that will halt replication of the cell through different pathways, in order to avoid proliferation of damaged cells (**Figure 6**). The response induced by p53 activation can vary based on severity and type of cellular stress. For instance the response can range from cell cycle arrest and DNA repair by p21 expression, to induction of the apoptotic cascade due to the expression of proteins BAX and PUMA (Vogelstein and Kinzler 2000). However missense mutations within the p53 gene (TP53) result in the following common six hotspots mutations or amino acid alterations in the protein: Arg-248, Arg-273, Arg-175, Gly-245, Arg-249, Arg-282, which occur in the DNA binding domain of p53 (Bullock and Fersht 2010), and thus adversely impact the protein's ability to bind DNA. Additionally, it has been found that these mutations result

in greatly decreased thermostability of the protein, and certain structural mutations can be made in order to increase this thermostability, however DNA-binding activity is not entirely rescued (Joerger *et al.* 2004). If p53 is unable to function as a transcription factor, damaged cells and cells carrying oncogenic mutations are able to avoid apoptosis and angiogenesis inhibition. Without these controls in place, these cancerous cells are able to replicate and proliferate, and eventually result in tumor growth and spread.

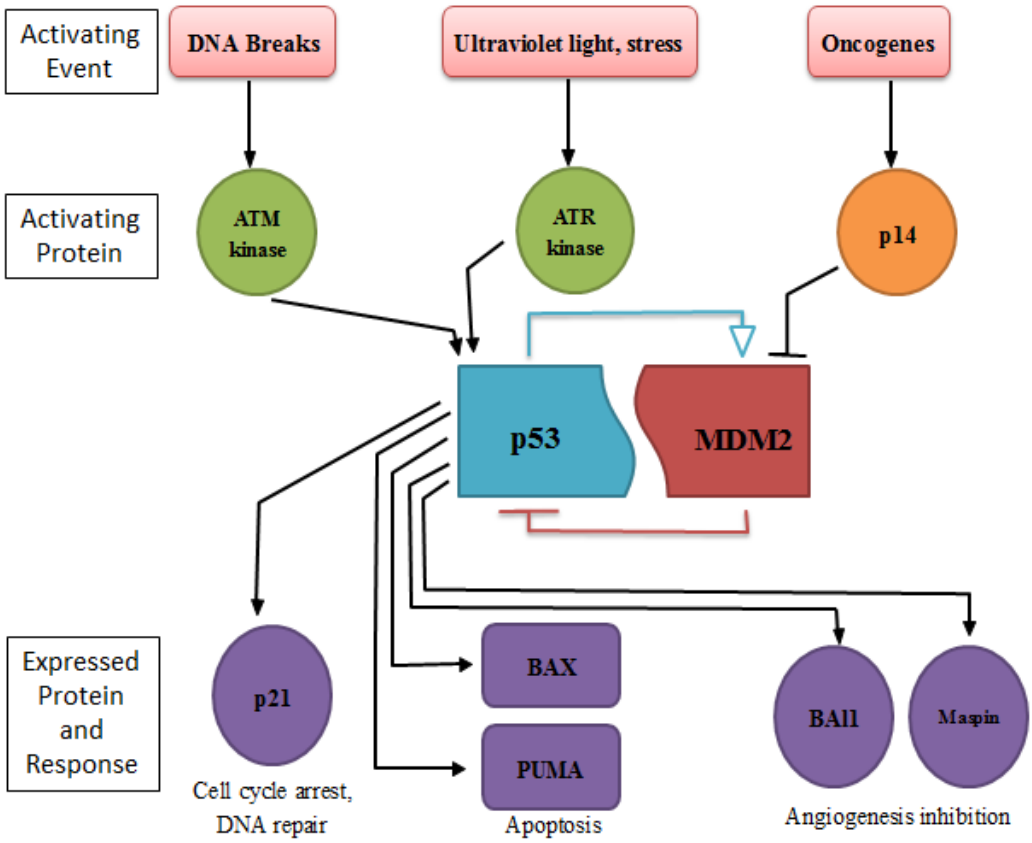

Figure 6. The p53 Pathway

In response to activating events such as DNA breaks and ultraviolet light or oxidative stress, ATM and ATR kinases (respectively) phosphorylate WT p53, thus activating it. MDM2 is a negative regulator of p53 that binds to the protein's transactivation domain, in order to inhibit it activation. Upregulation of p53 leads to MDM2 expression (in this way p53 is a self-regulator), MDM2 binding leads to degradation of p53 by the proteasome. However, elevated oncogene (such as Ras or MYC) signaling can lead to induction of p14, a negative regulator of MDM2, thus allowing for p53 activation. Once active p53 functions as a transcription factor, enabling the transcription and expression of proteins (in a time-dependent manner) such p21 (initially), which will induce cell cycle arrest allowing for the cell to evaluate the DNA damagae and determine if repair is viable. If it is not, elevated p53 (and persisting) levels will lead to the transcription and expression of proteins such as BAX and BAI1 which will respectively induce apoptosis and angiogenesis inhibition, in order to avoid the replication of damaged cells and reduce blood supply to the tumor (thus inhibiting its growth). Adapted from Sánchez 2016.

In addition to mutant p53's loss-of-function, which results in cancer pathogenesis, it is also believed that mutant p53 can lead to cancer pathogenesis through dominant-negative and gain-of-function pathways (Kim and An 2016). The dominant-negative effect of mutant p53 results from the mutated protein being able to complex with wildtype (WT) p53, thus inhibiting the binding of WT p53 to DNA. In addition, mutated forms are more likely to aggregate and thus tie up WT p53 monomers, resulting in a dominant-negative effect (Kim and An 2016). Finally it has been found that mutant p53 uniquely reacts with protein partners outside of the normal pathway, which describes the third pathway (gain-of-function) through which p53 can lead to cancer pathogenesis. One example of this is that mutant p53 serves functions outside of the nucleus, particularly in the mitochondria and endoplasmic reticulum (ER), including altering signaling in these organelles in order to evade apoptosis; for instance p53 mutants were unable to activate Bax and Bak within the mitochondria resulting in no cytochrome c release, thus avoiding apoptosis initiation, an extra-nuclear function that WT p53 serves (Giorgi *et al.* 2016). Another example is that mutant p53 has been found to uniquely interact with protein partners (non-transcriptional activity) and result in functions that actively promote tumor growth, such as complexing with nuclease MRE11 which results in genetic in-stability in tumors and pre-tumorigenic lesions in mouse models (Freed-Pastor and Prives 2012). Another example of mutant p53 gain-of-function, is the mutants unique ability to bind p53 homologs p63 and p73 which results in inhibition of p73-dependent apoptosis and chemosensitivity (Mantovani *et al.* 2016). Taken together, this evidence indicates that mutated p53 results in loss of the cell's viability through several mechanisms and thus

highlights the imperativeness of re-activating p53 WT activity. Due to these insights, p53 has been commonly called the "guardian of the genome" and the significance of the viability of this protein has become quite clear as it has been found to be mutated, in over fifty-percent of human cancers (Lukman *et al.* 2013). However other previously mentioned external factors can alter p53 activity, resulting in cancer pathogenesis as well.

MDM2 and MDM4 inhibition of Wildtype p53

Two specific factors that can affect the wild-type p53 pathway are MDM2 and MDM4. The MDM2 protein is responsible for the negative regulation (degradation) of p53 (**Figure 7**); and MDM2 expression is induced by p53 when the transcription factor is at high levels (Urso *et al.* 2016). MDM2 binds to the N-terminus of p53 thus occupying its transactivation domain and inhibiting its activation, then the complex is ubiquitinated and degraded by the proteasome. However elevated signaling from certain oncogenes (such as Ras or MYC) can lead to induction of p14, a negative regulator of MDM2, which degrades MDM2 allowing for activation of p53 (Vogelstein and Kinzler 2000). Another natural inhibitor of p53 activity is MDM4 (also known as MDMX). MDM4 is structurally similar to MDM2 and inhibits p53 activity by a similar mechanism, however its expression is not induced by p53 and it lacks the ubiquitin-ligase activity of MDM2 (Vogelstein and Kinzler 2000). Because of this if MDM2 and MDM4 are abnormally upregulated the tumor suppressive activity of p53 will also be inhibited (Urso *et al.* 2016). Ultimately one or more of these factors lead to the suppression of the overall p53 pathway in all human cancers.

Reactivation of Mutant p53

Due to the high correlation between inactivated p53 and cancer, the protein has been extensively studied as a potential therapeutic target for cancer in recent history. Mutant p53 reactivation, or the use of small molecules that bind to mutant p53 and stabilize its active confirmation, is currently being investigated as a potential cancer treatment in recent literature. One of the earliest examples of this kind of research involved the screening of over 100,000 compounds against p53 DNA binding domain (DBD) epitopes (Foster *et al.* 1999). Two hits were identified and studied as "prototype compounds". CP-31398 and CP-257042 were initially shown to bind to epitopes of the DBD of mutant p53 and improve the thermostability of protein in a dose-dependent manner (Foster *et al.* 1999). These prototype compounds were also shown to be able to conformationally modulate all of the four randomly chosen p53 mutants *in vitro* and functionally activate three mutants *in vivo*. This study utilized two different types of xenografts (A375.S2 melanoma cell line - mutated at p53 position 249 and DLD-1 colon carcinoma cell line - mutated at p53 position 241) which rapidly formed tumors in nude mice, and showed that CP-31398 slowed tumor growth by ~75% (twice daily injections at 100 mg/kg for 7 days) in the melanoma cell line, and that tumor growth was entirely inhibited in the colon carcinoma cell line with this dosing regimen (Foster *et al.* 1999). However the PK data of the lead compound (CP-31398) indicated that the dosing did not maintain the concentration of compound required for sustained p53 activity, and the authors noted that further optimization of the prototype compound would be required.

Another study identified a small molecule, SCH529074, with the ability to bind the DBD of p53, restore the growth-suppressive function of mutant p53, and interrupt the MDM2-mediated ubiquitination of WT p53 (Demma *et al.* 2010). The compound belonging to a class of piperazinyl-quiazolines, was shown to significantly increase the amount of p53 that binds to DNA and the protein's binding affinity (K_d) for DNA via a quantitative DNA binding assay in the case of two p53 mutants (Demma *et al.* 2010). Additionally, SCH529074 was able induce transcription of p53 dependent genes (p21 and bax) in a tumor cell line (H460 cells), and tumor regression in a human DLD-1 colorectal cancer xenograft model (30 mg/kg or 50 mg/kg given orally twice daily from day 3 until day 31) (Demma *et al.* 2010).

Another small molecule mutant p53 reactivator that initially showed great promise is Prima-1. It is compound that is currently in clinical trials and has been reported to reactivate mutant p53 in human cancer cells (Wiman 2010). However, this compound was later shown to be also working through mechanisms other than solely binding to mutant p53 (Cui *et al.* 2014), including forming covalent bonds with mutant p53 and causing apoptosis in p53 null cells (Lambert *et al.* 2009). This indicates that Prima-1 could induce toxicity in all cells, resulting in Prima-1 being a poor drug candidate; however, its clinical trials are still ongoing.

Another group's work has resulted in evidence supporting pharmacological reactivation of mutant p53 as a potential cancer therapy using a Cre-loxP-based strategy in order to temporally control tumor suppressor gene expression *in vivo* (Ventura *et al.* 2007). Their work indicated that restoring endogenous p53 expression leads to regression

of autochthonous lymphomas and sarcomas in mice without affecting normal tissues. However, they also found that the mechanism responsible for tumor regression is dependent on the tumor type. Their results indicated that the main consequence of p53 restoration was apoptosis in lymphomas, but suppression of cell growth (likely senescence) in sarcomas (Ventura *et al.* 2007). Taken altogether, these results suggest that pharmacological p53 reactivation may have utility as a potential therapeutic strategy for combating cancer.

RESEARCH OBJECTIVE

Since mutant p53 is a contributing factor in the case of many cancers, the goal of this study is to design compounds that bind to mutant p53 and restore its tumor suppressor function, with the hope that some of these compounds can be further optimized in order to eventually produce marketable drugs for anti-cancer therapies. So far numerous analogs have been synthesized within two major compound classes: benzimidazoles and quinolones (**Figure 7**) that have been shown to bind to, and restore the function of mutant p53 in cancer cells. The quinolone compound class was initially identified as inhibitors of a protease in the angiogenesis pathway (Liu *et al.* 2010). For this reason the Doll lab believed these compounds might be inhibiting angiogenesis by a different mechanism, such as by activating p53 instead. This hypothesis was confirmed through work of the Dasmahapatra lab, when these compounds were shown to induce transcription of p53-dependent genes in cancer cell lines with mutant p53. The benzimidazole structural class, was discovered to bind to mutant p53 via a scintillation-

proximity assay (Dasmahapatra and Demma 2007) and were later determined, by the Doll and Das labs, to induce expression of proteins downstream of the p53 pathway in cancer cell lines as well.

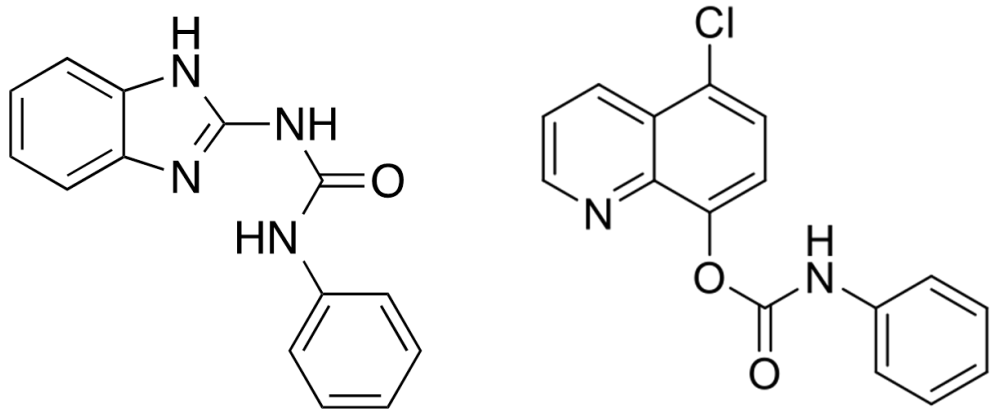

Figure 7. Benzimidazole and Quinolone structural classes
Compounds identified as p53-binders and –reactivators via work of Dr. Dasmahapatra and colleagues (Dasmahapatra and Demma 2007).

Previous research conducted by our lab has studied the effects of electronegativity of substituents on the metabolism of the given compound using an *in vitro* human liver microsomal protein assay (Sánchez 2016). It was found that the addition of an electron withdrawing group (fluorine) inhibited metabolism (human *in vitro* half-life increased from 15 ± 2.42 min. to 30 ± 2.06 min.) in accordance with literature (Kearns and Di 2011), while the addition of an electron donating group (methyl) increased the rate of metabolism (half-life decreased) (Sánchez 2016).

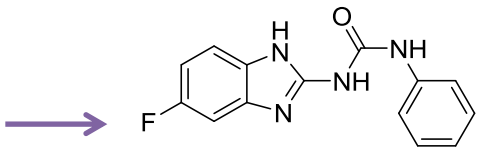

Figure 8. Previously studied Benzimidazole Urea with an electron-withdrawing group
Here the EWG is fluorine, depicted by purple arrow. Compound synthesized and studied by Stephanie Sánchez (RD 83).

The current study focused on determining the impact of steric size versus electronegativity of a substituent on the inhibition of *in vitro* human metabolism of our p53 reactivating compounds by the CYP450 enzymes contained in human liver microsomes. In previous research, inhibition of metabolism of these compounds was observed due to the addition of electron withdrawing groups on the metabolic site of the compounds (**Figure 8**) (Sánchez 2016), as predicted in the literature (Kearns and Di 2011). The goal of this study was to evaluate if the size (atomic radius) of the added substituent also has an effect on the metabolism of the compounds. To the best of our knowledge this avenue enhancing metabolic stability, through addition of various halogen substituents (other than fluorine), has not been investigated previously in the literature. While some of the studies discussed previously provide structural insights into the binding pockets and specificities of different CYP450 isozymes, the current study is unique and specific in scope, and focused in the specific context optimizing drug development through evaluation of drug-like properties. The synthesized compounds being examined in this study were incubated with human liver microsomes and the

metabolism of these compounds was followed using LC/MS to give intrinsic clearance values for each compound. Comparing the intrinsic clearance and half-life of our synthesized compounds will provide insight into the relative contribution of steric size and electronegativity towards metabolism inhibition.

EXPERIMENTAL METHODS

Background

Liquid Chromatography-Mass Spectrometry

Liquid chromatography-mass spectrometry (LC/MS) is an analytical technique that is utilized in many fields in order to separate and analyze components of mixtures. This system is comprised of two key units, the unit which carries out (high perfomance) liquid chromatography (HPLC) or the separation of compounds within the liquid sample, and the mass spectrometer (MS) which analyzes the separated components in order to determine their molecular weight. The general idea of this technique is that once a solution of the sample is taken up it is injected into the mobile phase which carries it through the chromatography column (stationary phase) and its components are separated based on their affinity to the stationary phase. These separated compounds then enter the mass spectrometer, undergo ionization and desolvation. The ions are then accelerated by high voltage electric fields through the mass analyzer. These ions move at different speeds to the detector based on their mass to charge ratio (m/z). The ion signals are then processed into mass spectra. Therefore the data provided is two-fold: HPLC chromatograms provide retention times of sample components (based on polarity) as well

as measurements of purity, while the mass analyzer provides mass spectra which indicate the molecular weight of ions (molecular weight of compound + proton due to ionization, results in M+1 peaks form parent compound) presence as well as their relative abundance. Additionally MS peak patterns for elements that have several isotopes with relatively high abundance (such as Cl and Br in this study) are well characterized and can provide further confirmation of structure characterization. An ultra-violet (UV) or another type of detector can also be added between the HPLC and the MS. The UV chromatogram is typically used a measure of compound purity and 95% or greater purity of a compound is required for proper characterization. Because of its broad utility, this technique has many applications. It is commonly used in drug discovery as a means of following synthesis reactions and characterizing compounds, however, it has also been used to quantitatively analyze compound concentrations in the metabolism and membrane transport studies, as described earlier.

The system utilized in this research has an ESI-TOF (electro-spray ionization, time of flight) mass analyzer, this means that components separated by the HPLC become ionized droplets through electro-spray, and are analyzed based on the time it takes for them to reach the detector, which relates to their mass to charge ratio (m/z). The HPLC of this system utilized an Analytical Echelon C18 analytical column (stationary phase) to separate samples with a mobile-phase gradient as depicted in **Table 4**.

Table 4. LC/MS Conditions

Analytical Echelon C18, 100X4.6 mm		
15 minute run		
Solvents: Water (A) / acetonitrile (B)		
Flow: 1.5 mL/min		
Time	**%A**	**%B**
0	70	30
1	70	30
8	30	70
9	30	70
11	20	80
12	15	85
13	70	30
15	70	30

Additionally our LC/MS generates two chromatograms: the UV detector provides the diode array chromatogram which is used in industry as means of measuring purity, while the more sensitive mass detector provides the total ion current (TIC) chromatogram.

Nuclear Magnetic Resonance Spectroscopy

Another spectroscopic technique employed in this research is nuclear magnetic resonance spectroscopy (NMR) which uses applied electric and magnetic fields in order determine the molecular structures on compounds. The two most common types of 1D NMR are C^{13}NMR and H^{1}NMR, however there are also more complex 2D experiments that can be run using an advanced system, and gives additional structural information. The instrument consists of a spinning sample-holder inside a super-conducting magnet, a

radio-frequency emitter and a receiver with a probe that goes inside the magnet to surround the sample, additionally gradient coils for diffusion measurements and electronics allow control and manipulation of the system. Spinning the sample is necessary to average out diffusional motion. Additionally use of a deuterated solvent is required since many solvents would contain NMR-sensitive protons. Since a constant magnetic field throughout the sample is required to detect small shifts in frequency, shims are used to adjust the homogeneity of the magnetic field. In order to further avoid inhomogeneity and drift in the magnetic field, the spectrometer uses a locking unit to maintain a lock on the solvent deuterium frequency. Shimming is adjusted automatically, though the shim parameters can be adjusted manually in order to attain the best resolution. Data collection begins, in the form of an individual free induction decay (FID), once the sample is excited with a radio frequency pulse. Additionally repeated acquisitions or scans can be averaged to improve the signal-to-noise ratio of the spectrum. A Fourier transform is carried out to extract, and then analyze, the spectrum from the raw FID.

This research utilized H^1NMR to characterize compounds. Samples were analyzed using a Bruker 400 MHz NMR and experiments were conducted with 16 scans in deuterated DMSO (DMSO-d6).

Synthetic Strategy

Scheme 1: General Pathway

Where R = Cl, Br, or I*

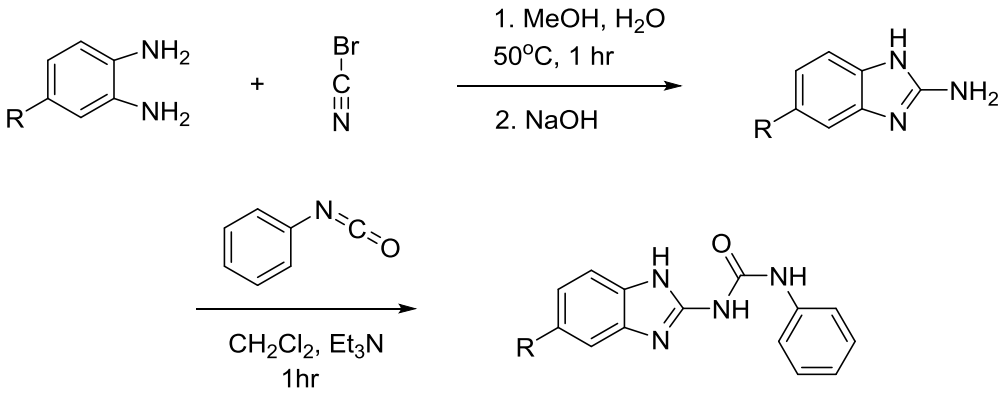

The synthetic procedure of the benzimidazole-urea compounds and their synthetic intermediates was described in a patent (Blackwell *et al.* 2013) titled *Inhibition and dispersion of bacterial biofilms with 2-aminobensimidazole derivatives* by Blackwell and colleagues, and was followed in this research. The general synthetic pathway is described in Scheme 1 which was followed for all compounds with the exception of the *Iodo-compound (RD98), which differed in terms of starting material and the initial reaction step as depicted in Scheme 4. The general synthetic strategy was that halogenated aminoanaline starting material was reacted with cyanogen bromide in order to cyclize the amine groups, in a 50:50 solvent mixture of methanol and water, which allows solubility of both reactants. Following the reaction the acidic side product, hydrobromic acid, is quenched using the base sodium hydroxide.

Scheme 2

Where R = Cl or Br

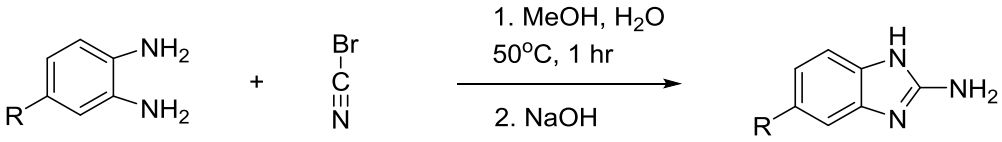

The purified and characterized intermediate was reacted with phenyl isocyanate using a catalytic amount trimethylamine in order to pull a proton off of the amine group of the intermediate, which increased its reactivity towards the carbon atom of the phenyl isocyanate. This reaction was performed in the solvent, dichloromethane, and had to be done in the absence of water, due to the fact that phenyl isocyanate could react with water to form a carbamate byproduct which inhibited the desired reaction, and was experienced early on in the synthetic process.

Scheme 3

Where R = Cl, Br, or I

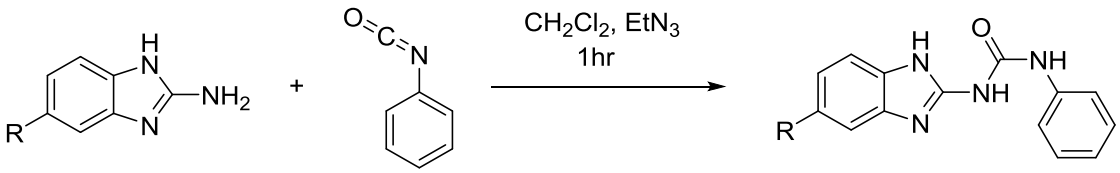

This synthetic strategy (Scheme 2) was initially followed for the Iodo- compound (using the Iodoaminoaniline starting material) however the reaction was not successful as

depicted by the impurity displayed in the chromatogram, indicated by the presence of multiple peaks, representing multiple chemically distinct molecules (**Figure 9**).

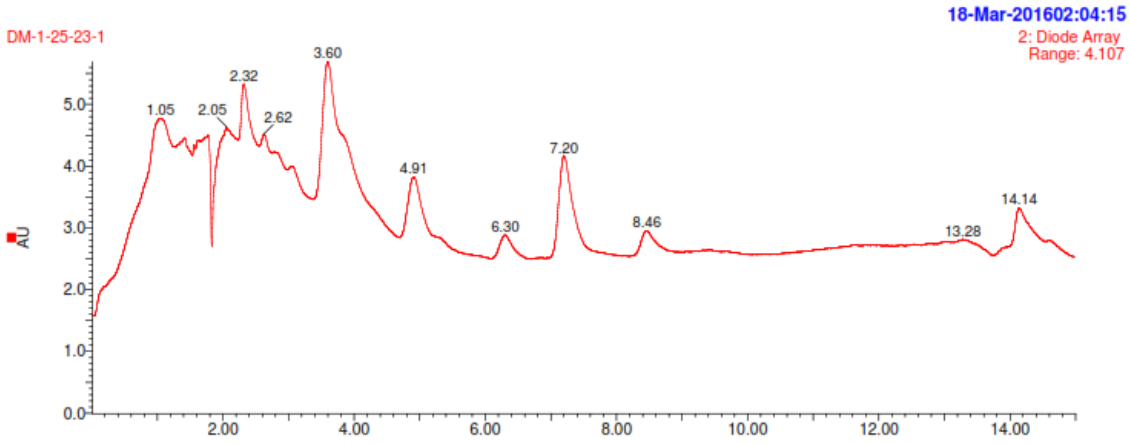

Figure 9. HPLC chromatogram of initial Iodo- reaction
Multiple peaks present after initial reaction and workup. Peak at 3.6 resembles some formation of desired product.

Therefore the purchased starting material was tested in order confirm its integrity, however it was found to be impure by LC/MS (**Figure 10**), indicated by multiple peaks in the UV chromatogram which suggests that the reactant degraded. From this evidence, it was concluded that the reaction failure was due to the prior degradation, and thus impurity, of the starting material.

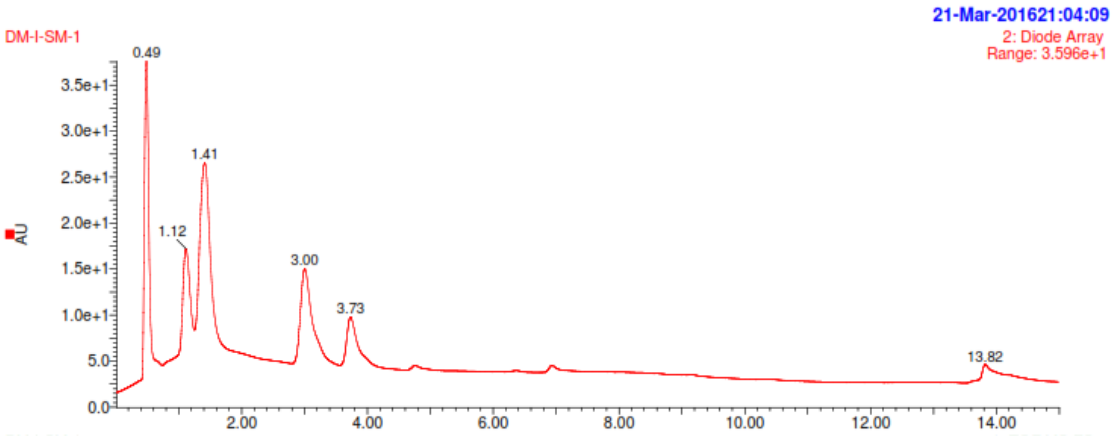

Figure 10. HPLC chromatogram of the Iodo-dianiline starting material
Multiple peaks indicate presence of multiple distinct compounds and therefore a great degree of impurity within the sample, presumably due to degradation.

After the failure of this reaction, the patent was revisited and found that solely for the Iodo- reaction, the researchers used an altered starting material (a nitroaniline instead of a aminoanaline as depicted in Scheme 4) presumably due to the unique instability of the Iodoaminoanaline. In this case, the Iodo-nitroaniline starting material was left to reflux in the solvent ethyl acetate with tin (II) chloride dehydrate for 12 hours in order to reduce the nitro- group of the starting material. After this step, the formed Iodo-dianaline is immediately reacted with cyanogen bromides, in order to avoid degradation, and the synthetic strategy follows the general synthetic pathway.

Scheme 4

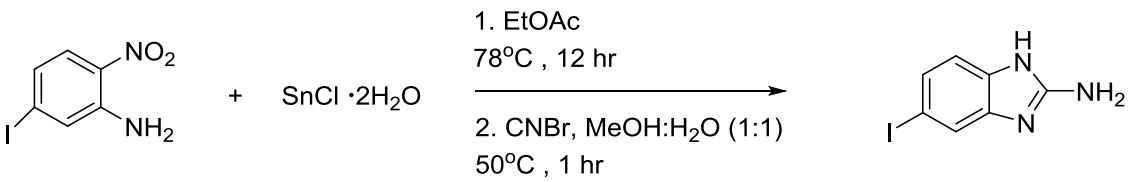

Reagents

All three Benzimidazole-Urea analogs were synthesized in the laboratory, supplied with reagents purchased from Sigma-Aldrich and Acros. Human liver microsomes (pooled male, 10mg/$190 used as is from BioreclamationIVT, 410-455-1242), and NADPH sources were purchased from Sigma-Aldrich as well.

Characterization

All synthesized compounds were characterized by nuclear magnetic resonance (NMR) and liquid chromatography coupled with mass spectroscopy (LC/MS) for purity and structure verification.

NMR spectra were recorded on a 400 MHz, Bruker instrument, TopSpin 2.1.6 Software, ICON-NMR 2.0 Automation Software with autosampler. Deuterated dimethyl sulfoxide (DMSO-d6) was used as a solvent for all NMR spectra. Chemical shifts were expressed in ppm (δ) relative to Tetramethylsilane (TMS), the accepted standard for calibrating chemical shift in NMR spectra. LC/MS were recorded on a Waters Time of Flight, Micromass LCT mass spectrometer coupled to an Agilent 1100 HPLC, with a syringe pump, API Probe and datastation MassLynx. The HPLC column was an Analytical, Echelon 100 x 4.6 mm C18 column with an acetonitrile (ACN)-water mobile phase flow rate of 1.5 mL/min and the following gradient: 0 min 30% ACN, 8 min 70% ACN, 9 min 70% ACN, 11 min 80% ACN, 12 min 85% ACN, 13 min 30% ACN, 15 min 30% ACN (see **Table 4**). Purified and characterized compounds were designated with "RD numbers", sequential numbers given to compounds from Ronald Doll's laboratory, and stored in glass containers at room temperature.

Synthetic Pathways

Scheme 1: General Pathway

Where R = Cl, Br, or I*

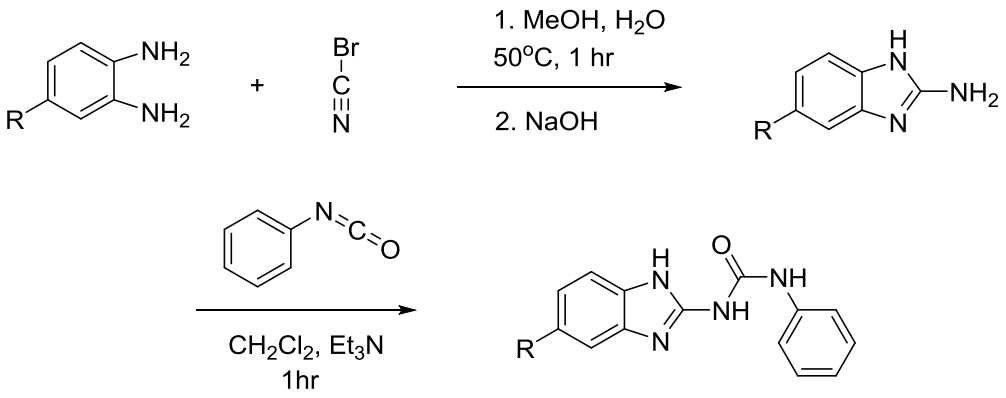

Synthesis of Intermediates:

Scheme 5

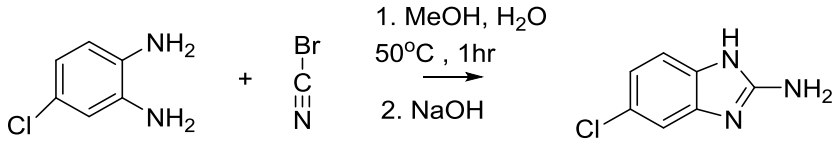

4-Chloro-2-aminobenzimidazole. ID#: DM-1-17-33. This intermediate was synthesized according to the US Patent Application #20130136782 (Blackwell *et al.* 2013). 4-chloro-phenylenediamine (1.0 g, 7.01 mmol, 1.0 equivalents) was dissolved in a 1:1 mixture of methanol (40 mL) and water (40 mL) in a 250mL round bottom flask. The reaction mixture was treated with cyanogen bromide (SIGMA, 2.2 g, 21.04 mmol, 3 eq.) and heated at 50°C for one hour and 45 minutes. After cooling to room temperature, the reaction mixture was concentrated under vacuum. The remaining mixture was basified

with 1.0 M aqueous NaOH until pH>8.0, and extracted with ethyl acetate (3x30 mL). The remaining organic mixture was washed with water (2x50 mL), saturated sodium chloride solution (50 mL), dried over $MgSO_4$ and concentrated under vacuum to yield 5-chloro-2-aminobenzimidazole. The product was then triturated with three portions of hexanes (3x10 mL) to yield (0.93±0.01)g of a brown solid that was used without further purification (Scheme 5).

Percent yield: 79.5%

m/z: . 167.85 (100%)

Percent purity by HPLC: 100%

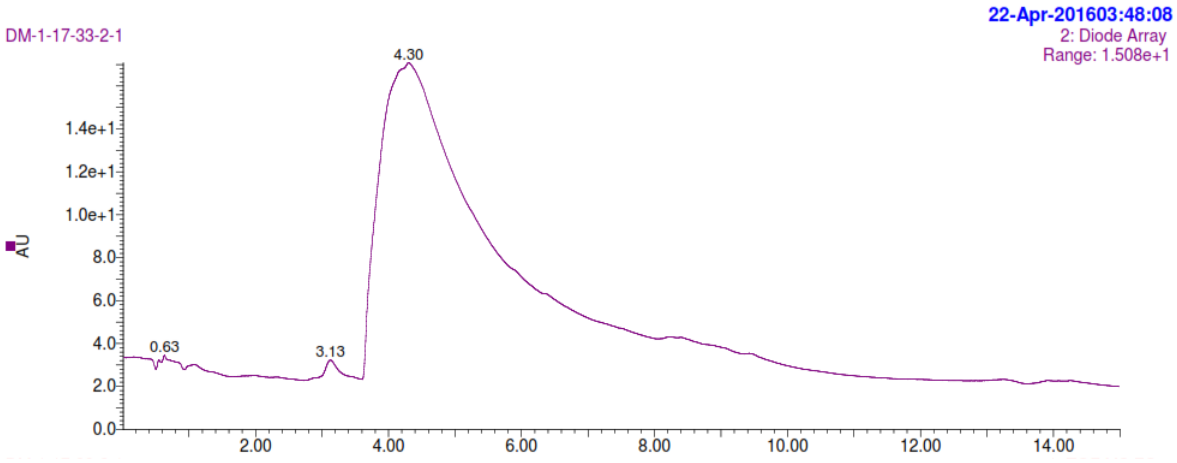

Figure 11. HPLC chromatogram of 4-chloro-2-aminobenzamidazole
Singular peak indicates a single compound in the sample, peak integration/purity readout indicates 100% purity of sample.

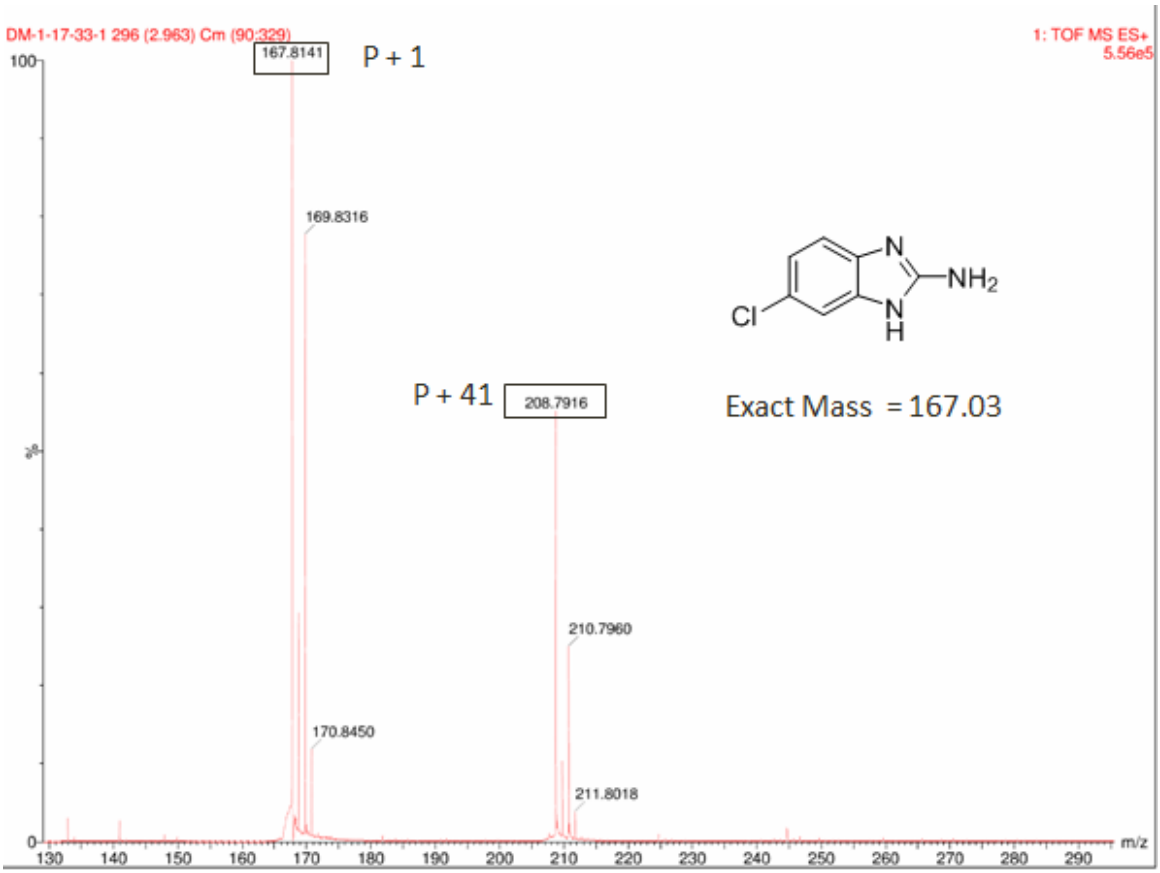

Figure 12. Mass Spectrum of 4-chloro-2-aminobenzamidazole
P+1 is the molecular ion +1, while the P+ 41 is M+ Acetonitrile indicating parent compound in complex with acetonitrile (solvent). Parent ion defined. Product had 100% purity via UV chromatogram.

Scheme 6

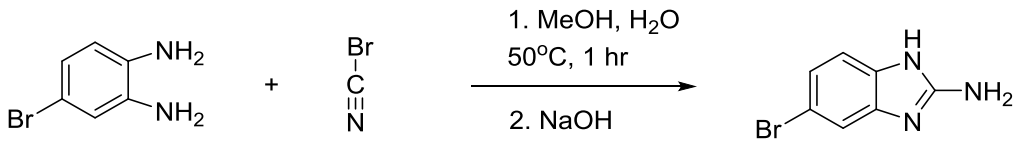

4-Bromo-2-aminobenzimidazole. ID#: DM-1-14-29. This intermediate was synthesized according to the US Patent Application #20130136782 (Blackwell *et al.* 2013). 4-bromo-1,2-diaminobenzene (1.0 g, 5.35 mmol, 1.0 eq.) was dissolved in a 1:1 mixture of

methanol (40 mL) and water (40 mL) in a 250mL round bottom flask. The reaction mixture was treated with cyanogen bromide (SIGMA, 1.7 g, 16.03 mmol, 3 eq.) and heated at 50°C for one hour and 45 minutes. After cooling to room temperature, the reaction mixture was concentrated under vacuum. The remaining mixture was basified with 1.0 M aqueous NaOH until pH>8.0, and extracted with ethyl acetate (3x30 mL). The remaining organic mixture was washed with water (2x50 mL), saturated sodium chloride solution (50 mL), dried over $MgSO_4$ and concentrated under vacuum to yield 5-chloro-2-aminobenzimidazole. The product was then triturated with three portions of hexanes (3x10 mL) to yield (0.91±0.01)g of a brown solid that was used without further purification (Scheme 6).

Percent yield: 82.7%

m/z: 211.68 (100.0%)

Percent purity by HPLC: 100%

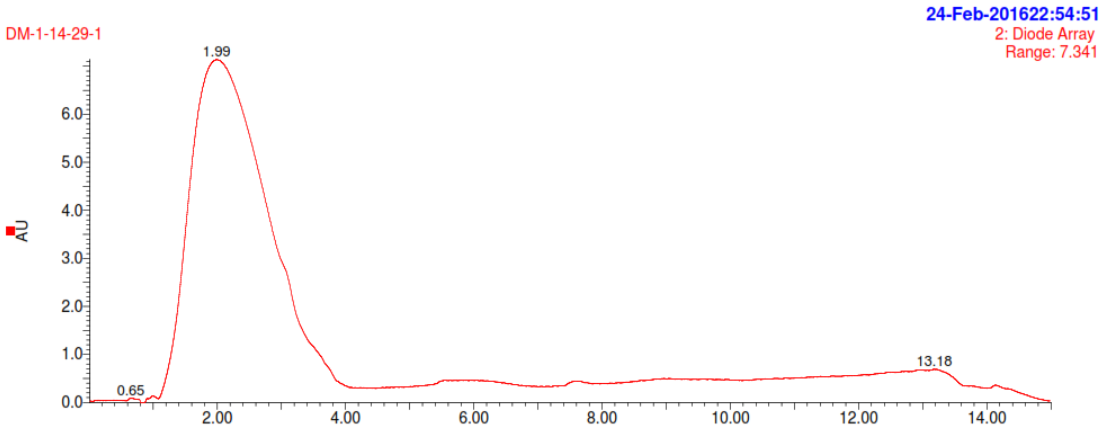

Figure 13. HPLC chromatogram of 4-bromo-2-aminobenzamidazole
Singular peak indicates a single compound in the sample, peak integration/purity readout indicates 100% purity of sample.

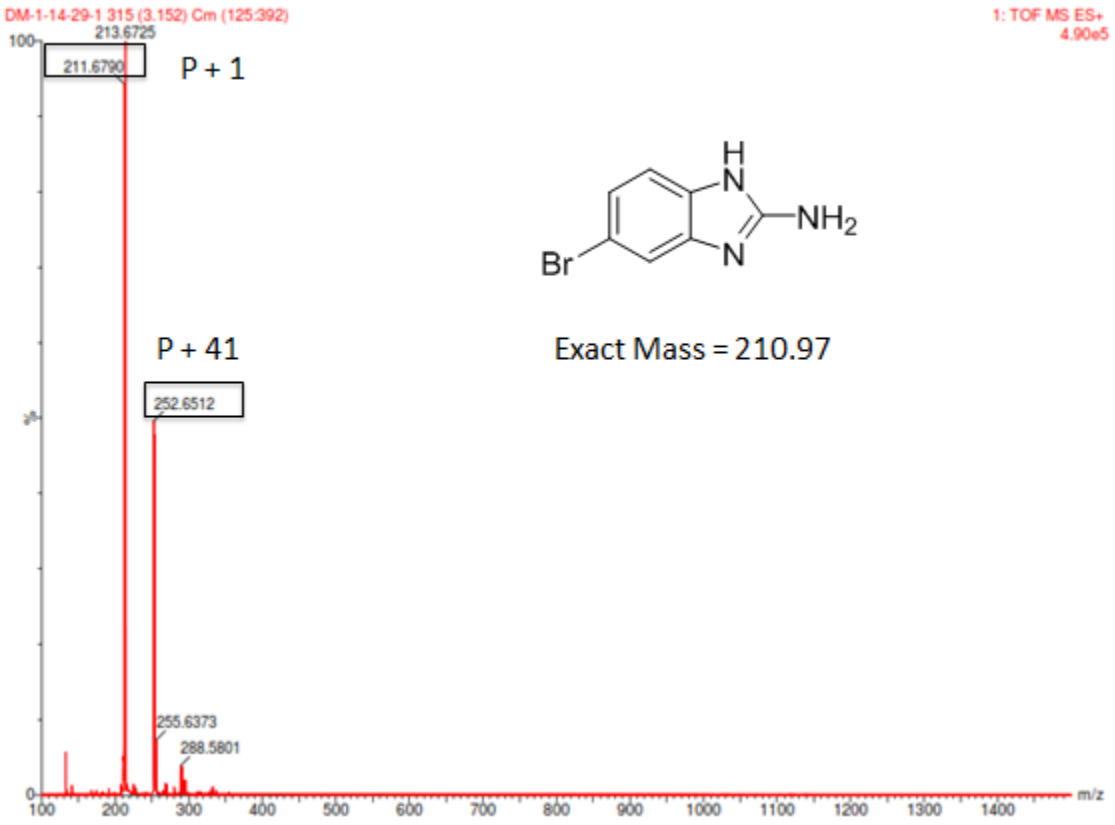

Figure 14. Mass Spectrum of 4-bromo-2-aminobenzamidazole
P+ 41 peak refers to ionized parent compound in complex with acetonitrile (solvent). Parent ion defined. Product had 100% purity via UV chromatogram.

Scheme 4

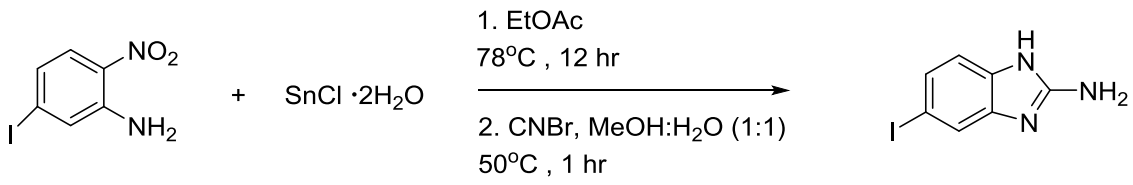

4-Iodo-2-aminobenzimidazole. ID#: DM-1-73-20. This intermediate was synthesized according to the US Patent Application #20130136782 (Blackwell *et al.* 2013). A 100mL round bottom flask was charged with 4-iodo-2-nitroaniline (0.88 g, 3.34 mmol, 1 eq.), tin (II) chloride dehydrate (3.76 g, 16.7 mmol, 5 eq.), and ethyl acetate (50 mL). The reaction mixture was left to reflux at 78°C for 12 hours.

Reaction mixture was cooled to room temperature and saturated with sodium bicarbonate (3 x 30 mL). Combined aqueous layers were washed with ethyl acetate (2 x 30 mL) and all organic layers were collected and concentrated under vacuum.

Resulting solid, 4-iodo-phenylenediamine (0.78 g, 3.34 mmol, 1.0 eq.) was dissolved in a 1:1 mixture of methanol (40 mL) and water (40 mL) in a 250mL round bottom flask. The reaction mixture was treated with cyanogen bromide (SIGMA, 1.19 g, 10.02 mmol, 3 eq.) and heated at 50°C for 1.5 hours. After cooling to room temperature, the reaction mixture was concentrated under vacuum. The remaining mixture was basified with 1.0 M aqueous NaOH until pH>8.0, and extracted with ethyl acetate (3x30 mL). The remaining organic mixture was washed with water (2x50 mL), saturated sodium chloride solution (50 mL), dried over $MgSO_4$ and concentrated under vacuum to yield 5-chloro-2-aminobenzimidazole. The product was then triturated with three portions of hexanes

(3x10 mL) to yield (0.44±0.01)g of a red-brown solid that was used without further purification (Scheme 4).

Percent yield: 51.0%

m/z: 261.01 (86.0%)

Percent purity by HPLC: 86%

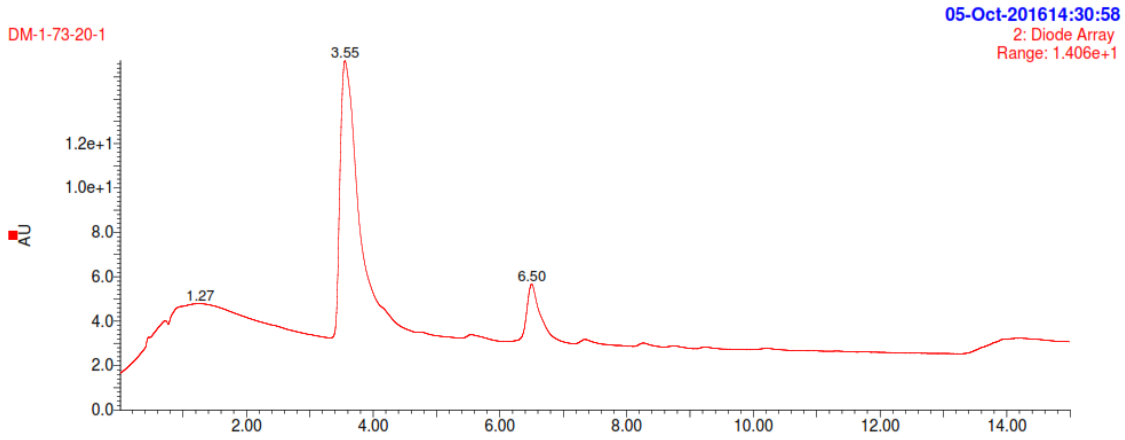

Figure 15. HPLC chromatogram of 4-iodo-2-aminobenzamidazole
The presence of two peaks indicate that two unique chemicals are present in the sample. Larger was found to be desired product (see MS provided below, Figure 17). Peak integration/purity readout indicates that sample purity is 86% of component with larger peak (RT of 3.55 min) and 14% of component with smaller peak (RT of 6.50 min). However second synthetic step was carried out using this sample (since it was mostly pure and its synthesis was involved) and 100% purity was achieved for final product (see Figure 24).

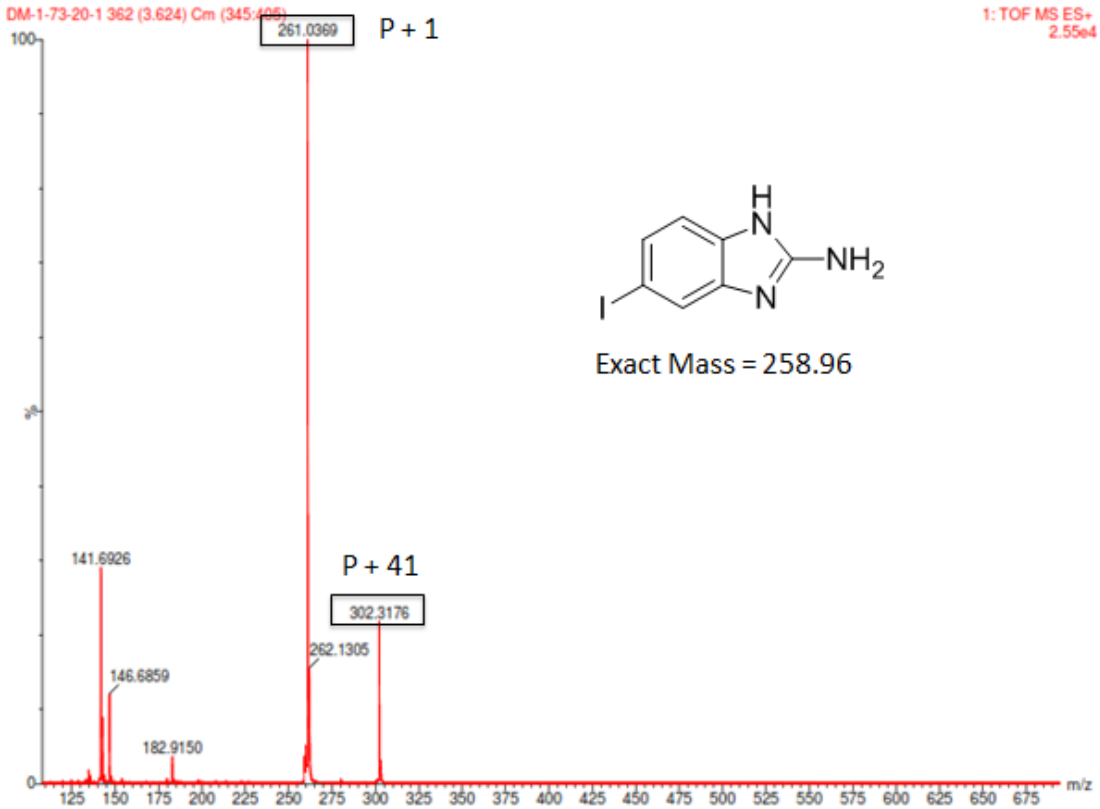

Figure 16. Mass Spectrum of 4-iodo-2-aminobenzamidazole
P+ 41 ion refers to parent compound in complex with acetonitrile (solvent). Parent ion defined. Unable to define ion a t 141.7. Product had 100% purity via UV chromatogram.

Synthesis of Final Products:

Scheme 7

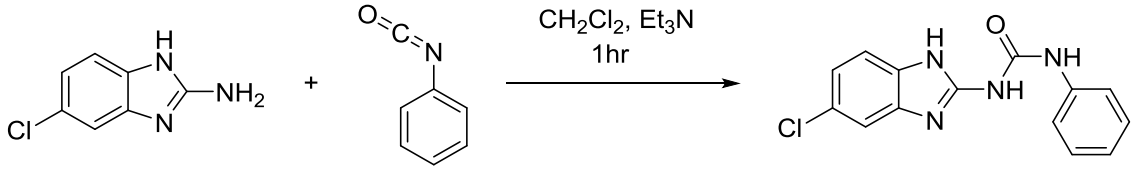

1-(6-Chloro-1H-benzo[d]imidazole-2-yl)-3-phenylurea: RD 88. ID#: DM-1-27-35. A 100ml round bottom flask was charged with 5-chloro-2-aminobenzimidazole (0.2 g, 1.19 mmol) and dissolved in 12 mL dichloromethane (CH_2Cl_2). To the resulting mixture, 3 drops triethylamine (Et_3N) was added along with phenyl isocyanate (0.15 mL, 1.19 mmol), both in excess. The reaction was allowed to stir overnight. The solution was washed with CH_2Cl_2 and transferred into a separatory funnel. Aqueous sodium bicarbonate was added and the organic layer was then separated. The remaining organic solution was washed with saturated sodium chloride solution and water. The solution was concentrated under vacuum. Recrystallization was performed using acetonitrile to yield (0.2±0.01) g of a red crystalline solid (Scheme 7).

Percent yield: 49.0%

m/z: 287.24 (100.0%)

NMR 400 mHz, ^{1}H NMR, DMSO: 9.47 ppm (1 H); 8.64 ppm (1 H, s, 5); 7.55 ppm (2 H, d, 3,p); 7.37 ppm (5 H, m, o,m,2).

Percent purity by HPLC: 100%

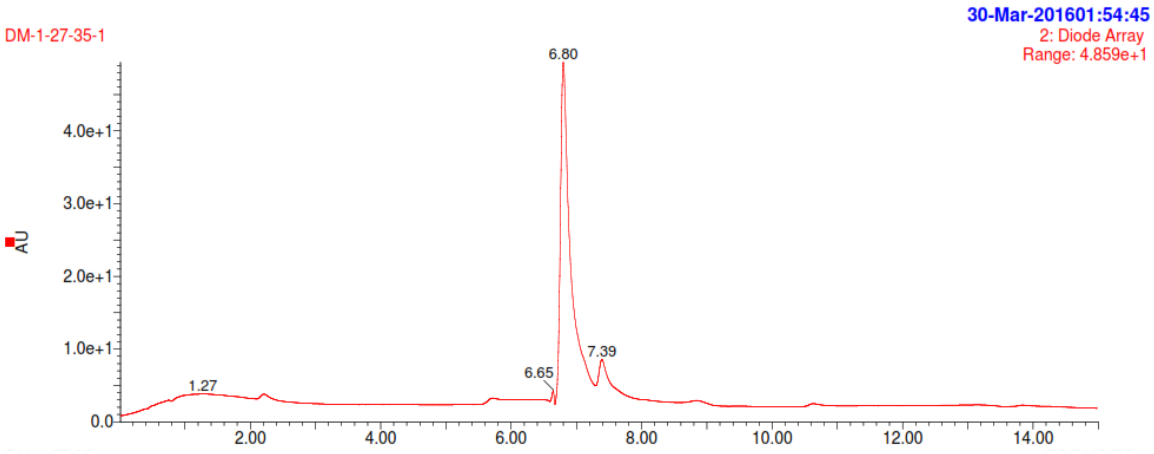

Figure 17. HPLC chromatogram of the 1-(6-Chloro-1H-benzo[d]imidazole-2-yl)-3-phenylurea
Singular peak indicates a single compound in the sample, peak integration/purity readout indicates 100% purity of sample.

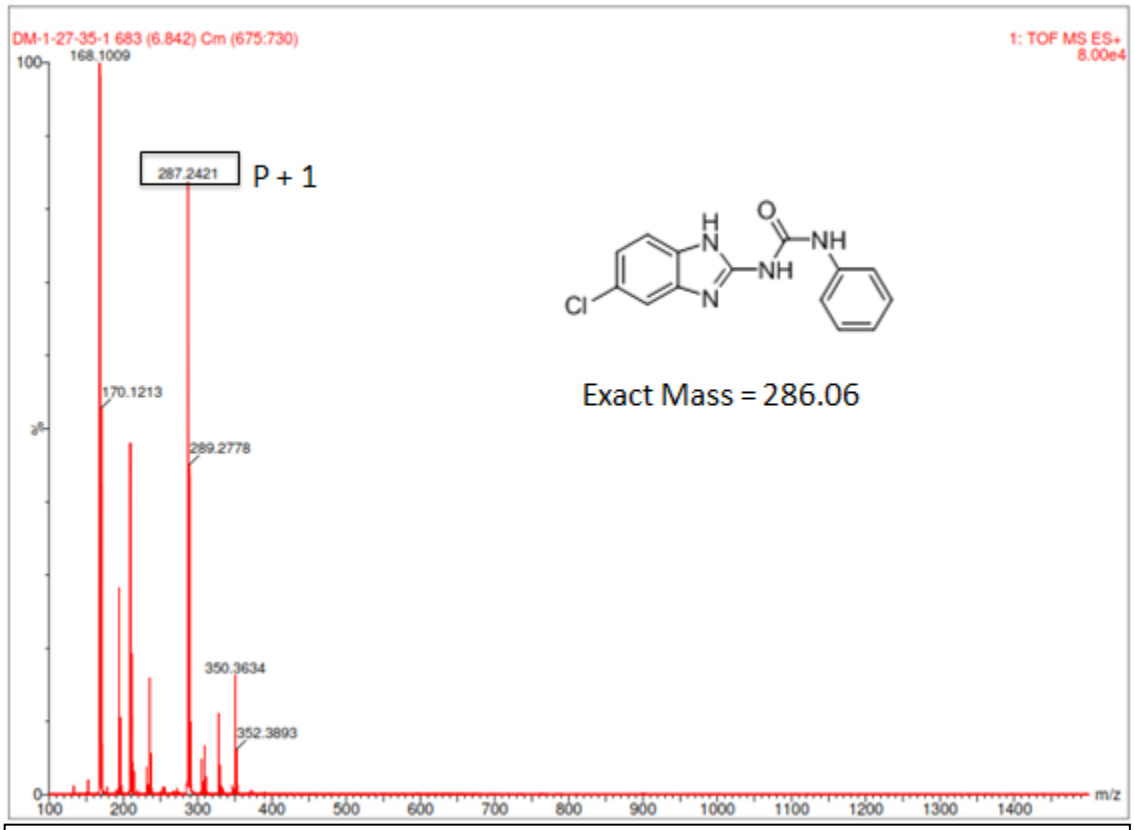

<u>Figure 18.</u> Mass spectrum of 1-(6-Chloro-1H-benzo[d]imidazole-2-yl)-3-phenylurea
Parent ion defined. Ion at 168.1 represents fragment (5-chloro-2-aminobenzimidazole). Product had 100% purity via UV chromatogram.

A

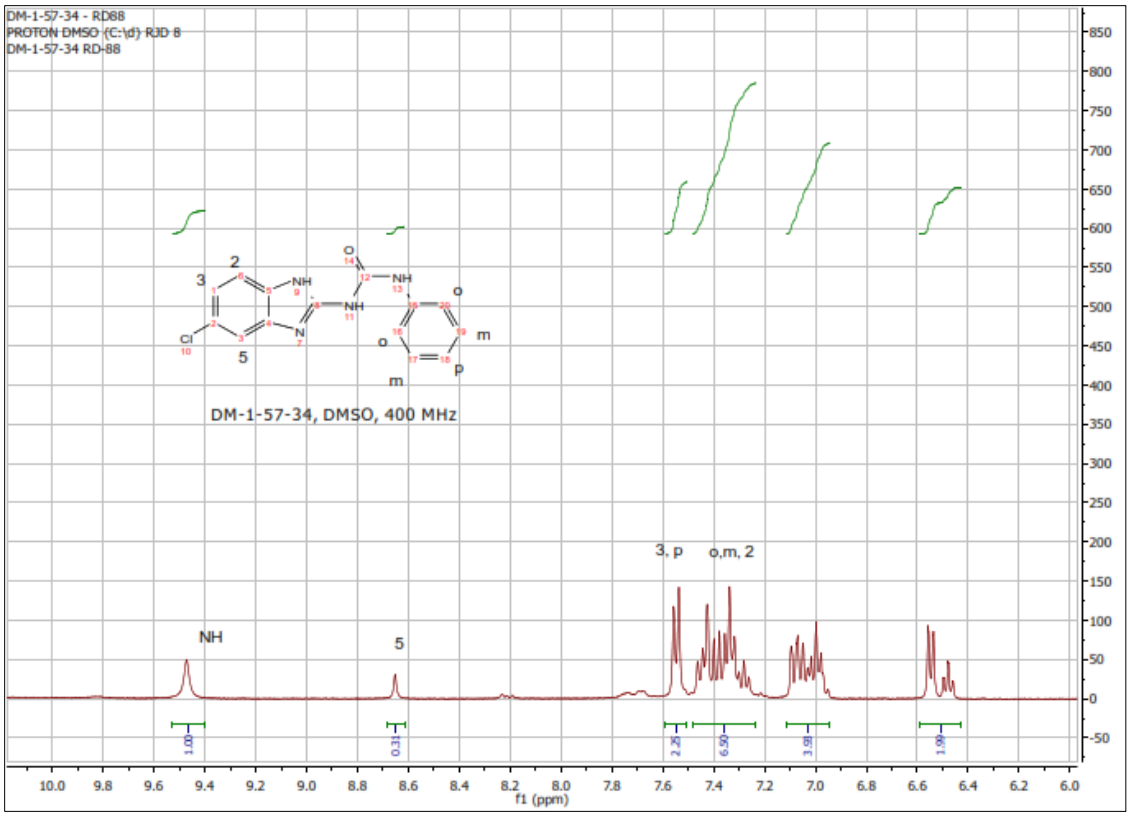

B

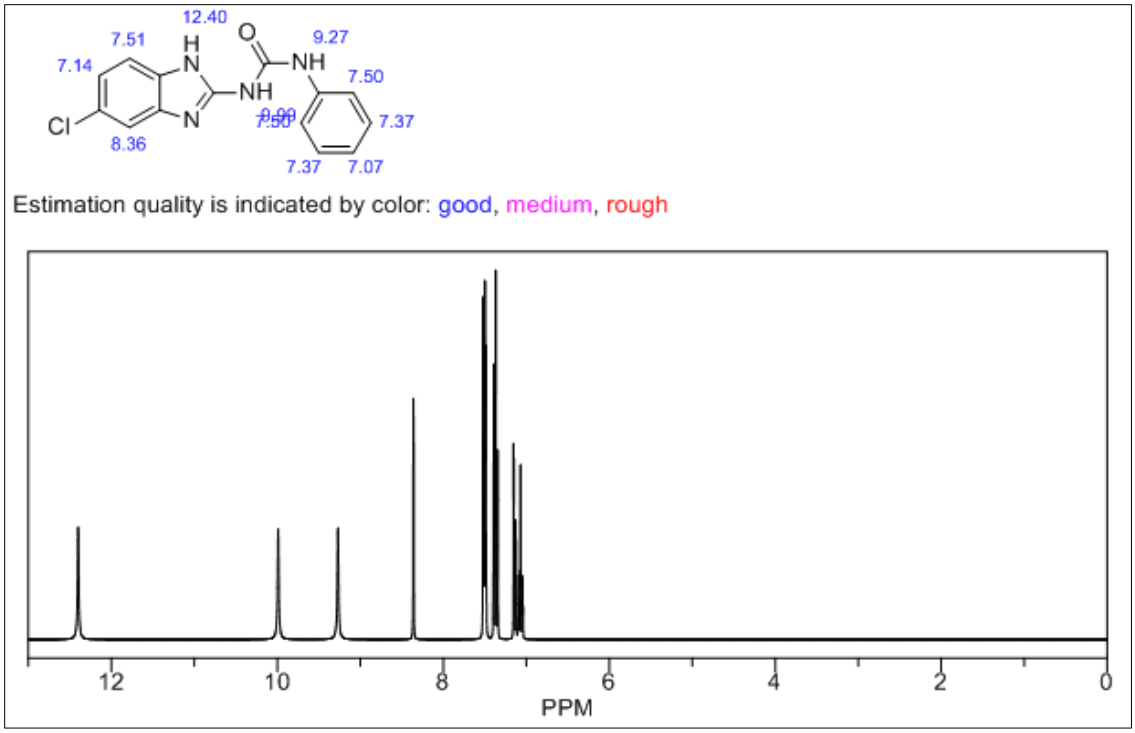

<u>Figure 19.</u> Proton NMR of 1-(6-Chloro-1H-benzo[d]imidazole-2-yl)-3-phenylurea in DMSO

A. Blowup of region of interest, solvent peaks not shown. Peaks assigned based on predicted chemical shifts (in DMSO via ChemDraw **B**)

Scheme 8

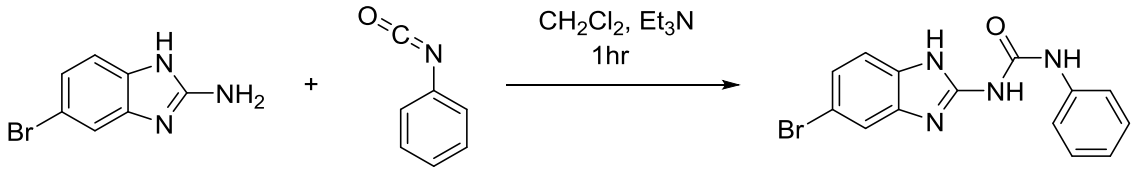

1-(6-Bromo-1H-benzo[d]imidazole-2-yl)-3-phenylurea: RD 97. ID#: DM-1-62-2. A 100ml round bottom flask was charged with 4-Bromo-2-aminobenzimidazole (0.3 g, 1.41 mmol) and dissolved in 12 mL CH_2Cl_2. To the resulting mixture, 3 drops of Et_3N was added along with phenyl isocyanate (0.175 mL, 1.41 mmol), both in excess. The reaction was allowed to stir overnight. The solution was washed with CH_2Cl_2 and transferred into a separatory funnel. Aqueous sodium bicarbonate was added and the organic layer was then separated. The remaining organic solution was washed with saturated sodium chloride solution and water. The solution was concentrated under vacuum. Recrystallization was performed using acetonitrile to yield (0.2±0.01) g of a tan solid (Scheme 8).

Percent yield: 42.0%

m/z: 332.39 (100.0%)

NMR 400 mHz, ^{1}H NMR, DMSO: 9.46 ppm (1 H); 7.54 ppm (3 H, d, o,5); 7.34 ppm (3 H, t, m,2); 7.20 ppm (1 H, d, 3); 7.04 ppm (1 H, t, p).

Percent purity by HPLC: 100%

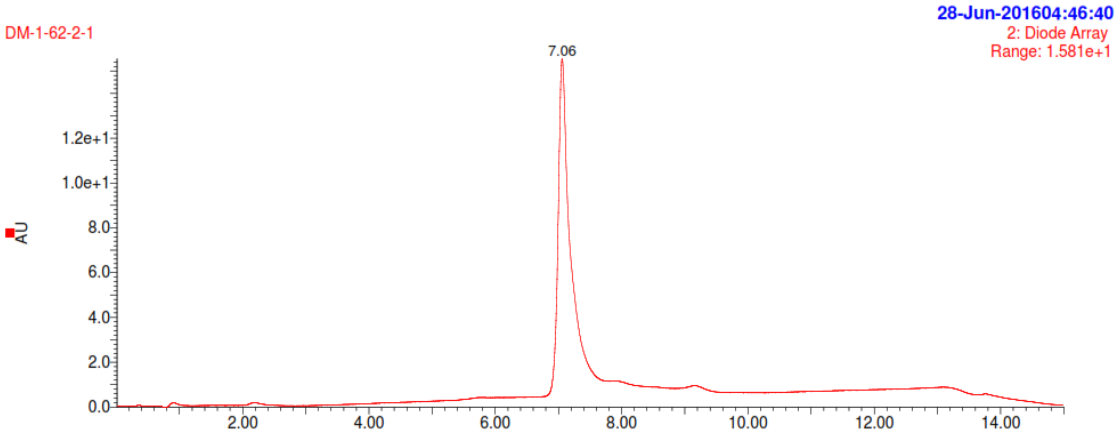

Figure 20. HPLC chromatogram of the 1-(6-Bromo-1H-benzo[d]imidazole-2-yl)-3-phenylurea
Singular peak indicates a single compound in the sample, peak integration/purity readout indicates 100% purity of sample.

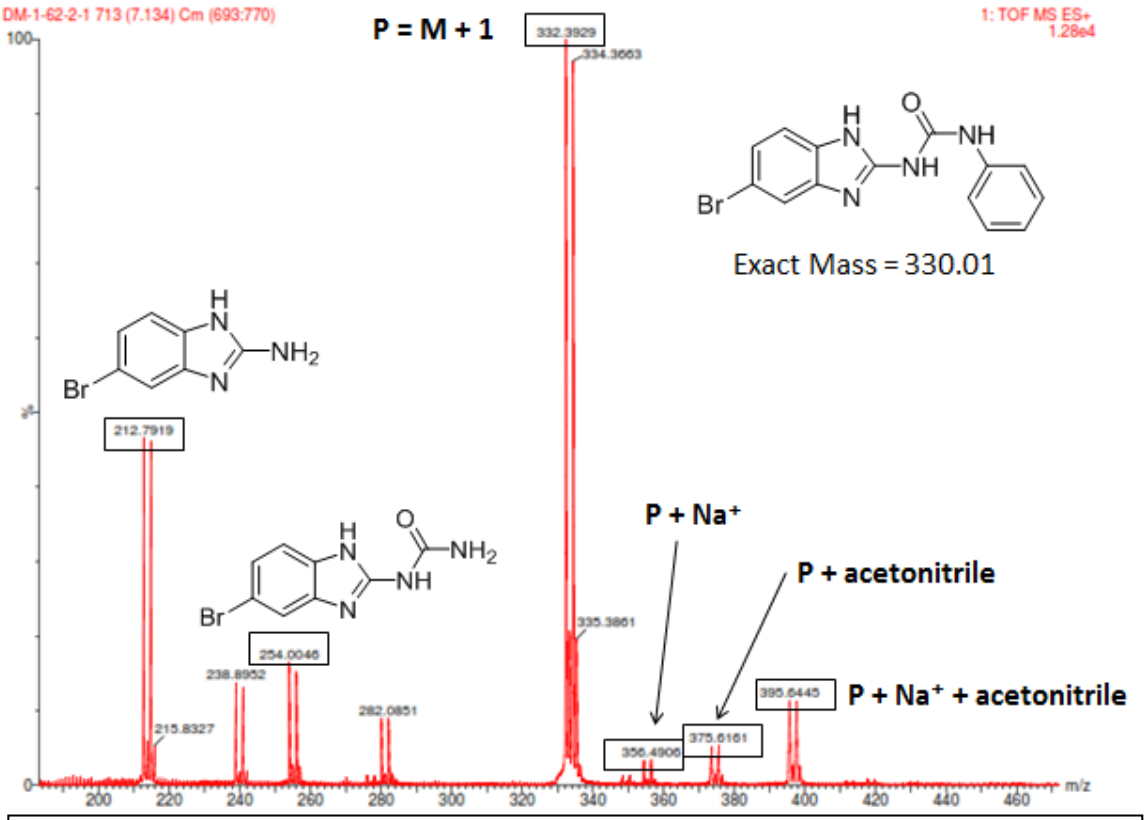

<u>Figure 21.</u> Mass spectrum of 1-(6-Bromo-1H-benzo[d]imidazole-2-yl)-3-phenylurea
Parent ion defined. Non-covalent complexes defined (P+23, P+41, and P+23+41 respectively). Fragments of greater intensity were defined as well (at 212.8 and 254.0). Product had 100% purity via UV chromatogram.

A

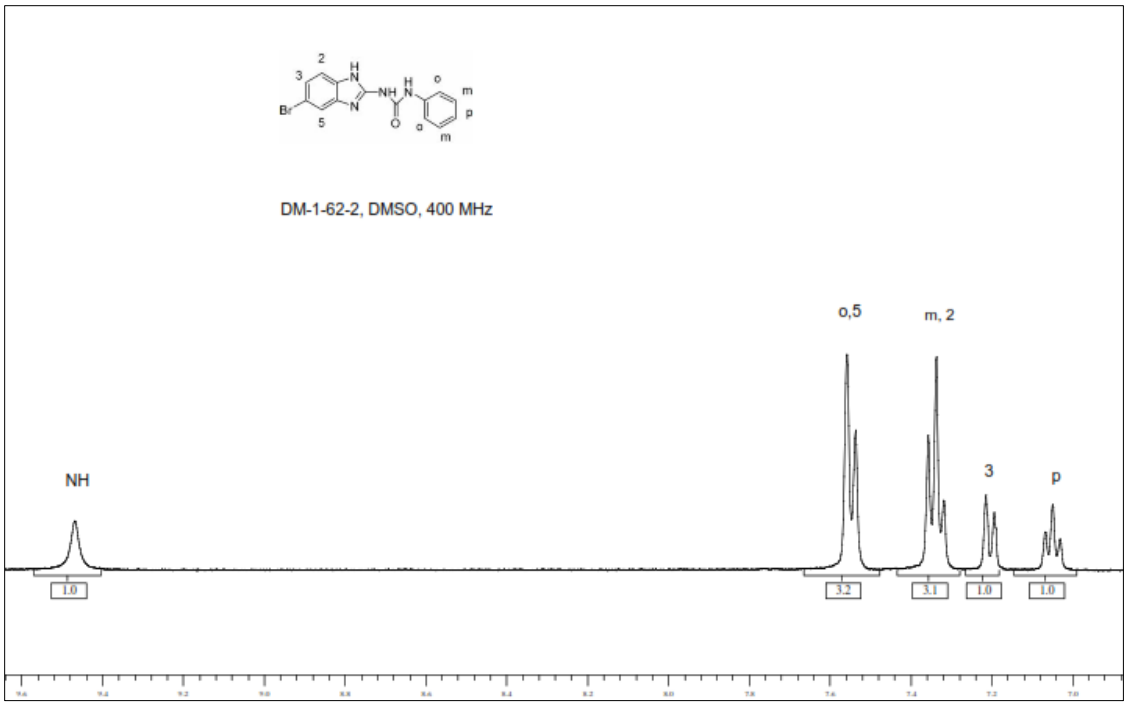

B

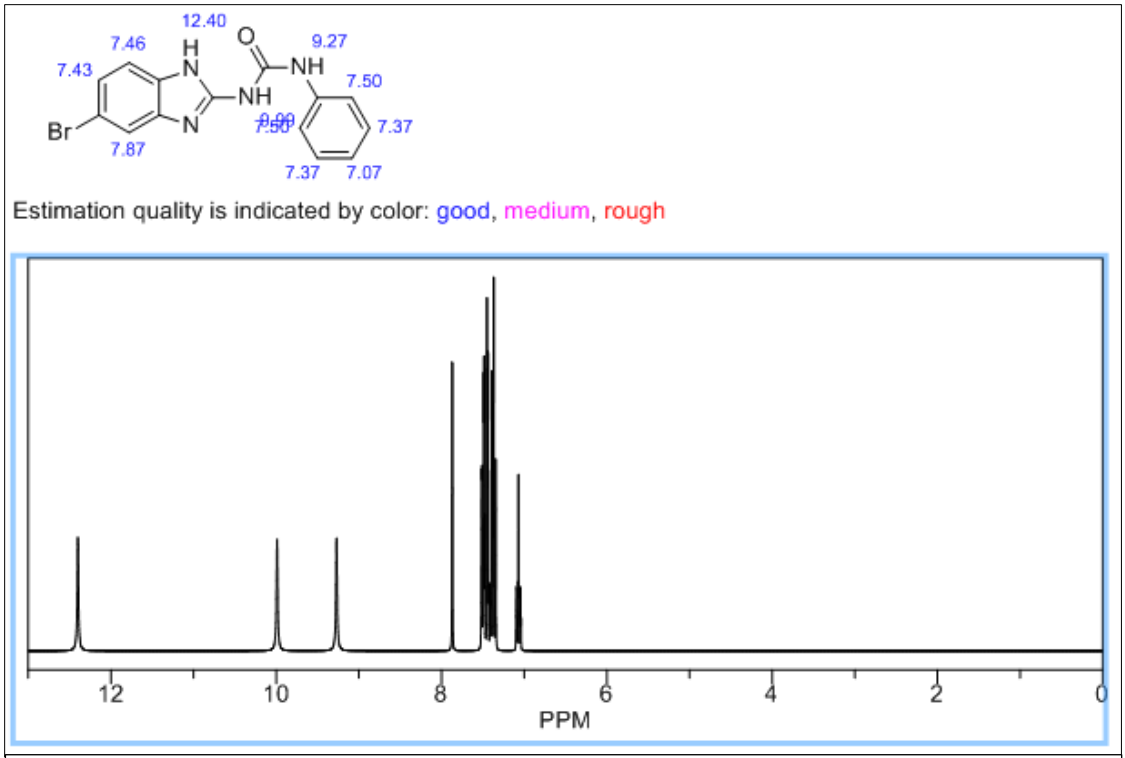

<u>Figure 22.</u> Proton NMR of 1-(6-Bromo-1H-benzo[d]imidazole-2-yl)-3-phenylurea in DMSO

A. Blowup of region of interest, solvent peaks not shown. Peaks assigned based on predicted chemical shifts (in DMSO via ChemDraw **B**)

Scheme 9

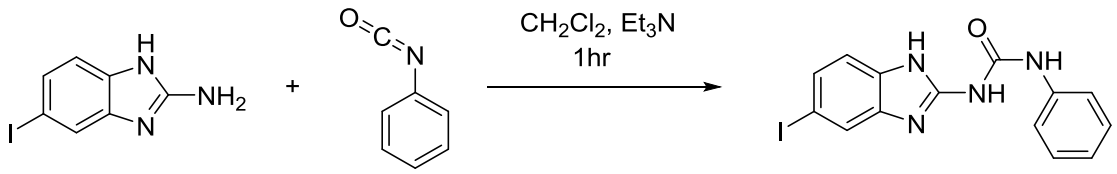

1-(6-Iodo-1H-benzo[d]imidazole-2-yl)-3-phenylurea: RD 98. ID#: DM-1-75-35(-C). A 100ml round bottom flask was charged with 5-idod-2-aminobenzimidazole (0.38 g, 1.467 mmol) and dissolved in 12 mL CH_2Cl_2. To the resulting mixture, 3 drops of Et_3N was added along with phenyl isocyanate (0.2 mL, 1.467 mmol), both in excess. The reaction was allowed to stir overnight. The solution was washed with CH_2Cl_2 and transferred into a separatory funnel. Aqueous sodium bicarbonate was added and the organic layer was then separated. The remaining organic solution was washed with saturated sodium chloride solution and water. The solution was concentrated under vacuum. Recrystallization was performed using acetonitrile to yield (0.44±0.01) g of a dark brown solid (Scheme 9).

Percent yield: 51.0%

m/z: 379.31 (100.0%)

NMR 400 mHz, ^{1}H NMR, DMSO: 9.49 ppm (1 H); 7.70 ppm (1 H, s, 5); 7.60 ppm (2 H, d, 2, 3); 7.35 ppm (5 H, m, o,m,p).

Percent purity by HPLC: 100%

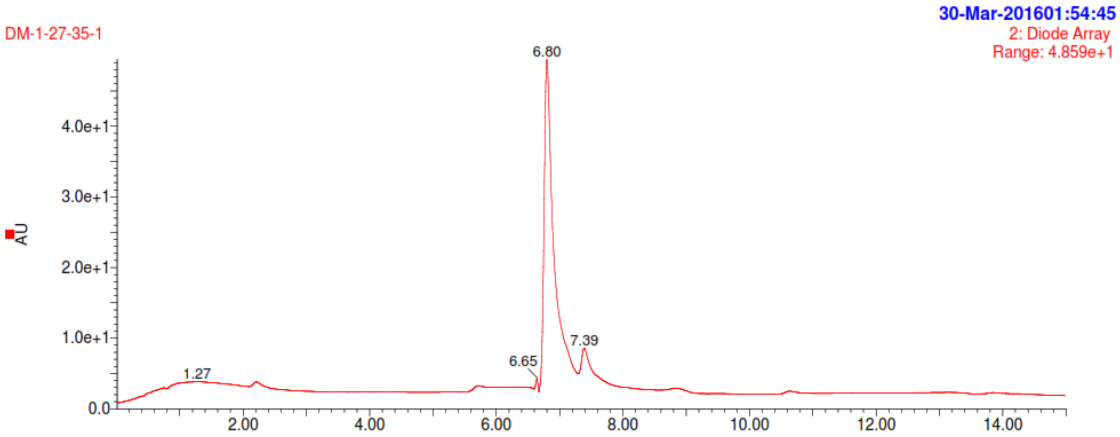

Figure 23. HPLC chromatogram of the 1-(6-Iodo-1H-benzo[d]imidazole-2-yl)-3-phenylurea
Singular peak indicates a single compound in the sample, peak integration/purity readout indicates 100% purity of sample.

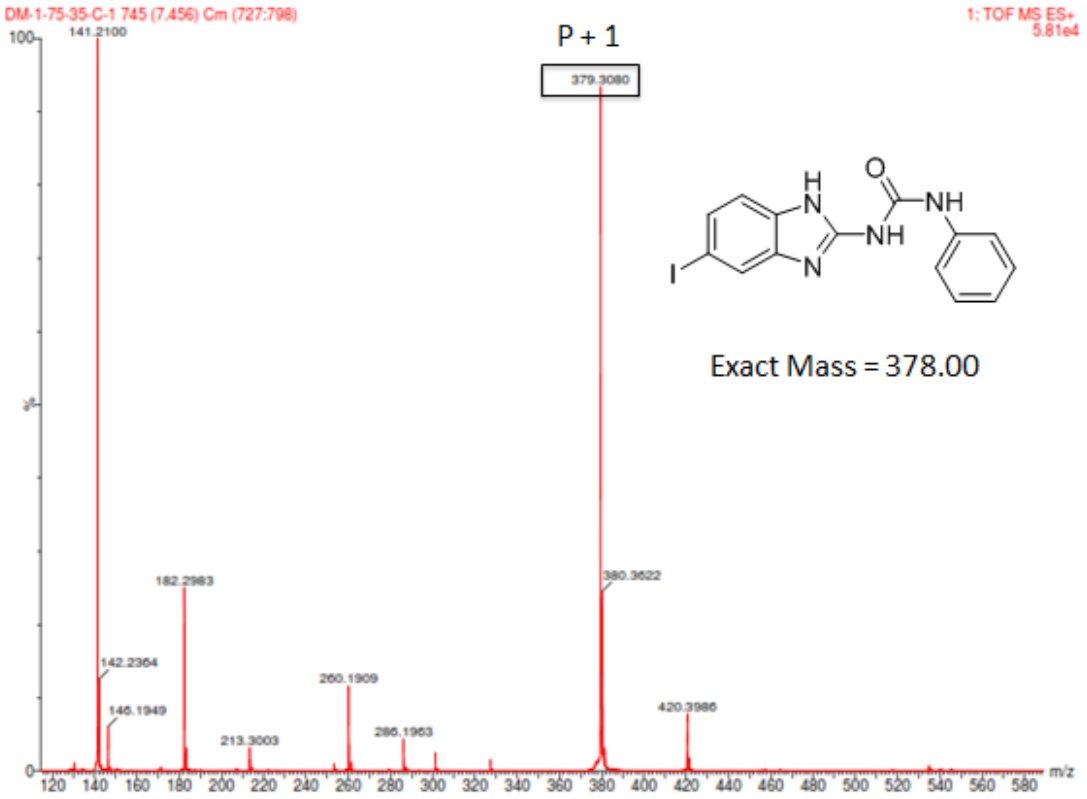

<u>Figure 24.</u> Mass spectrum of 1-(6-Iodo-1H-benzo[d]imidazole-2-yl)-3-phenylurea
Parent ion defined. Ion at 420.4 represents complex of P + acetonitrile. Unable to define ion at 141.2 (however common ion with Iodo intermediate). Product had 100% purity via UV chromatogram.

A

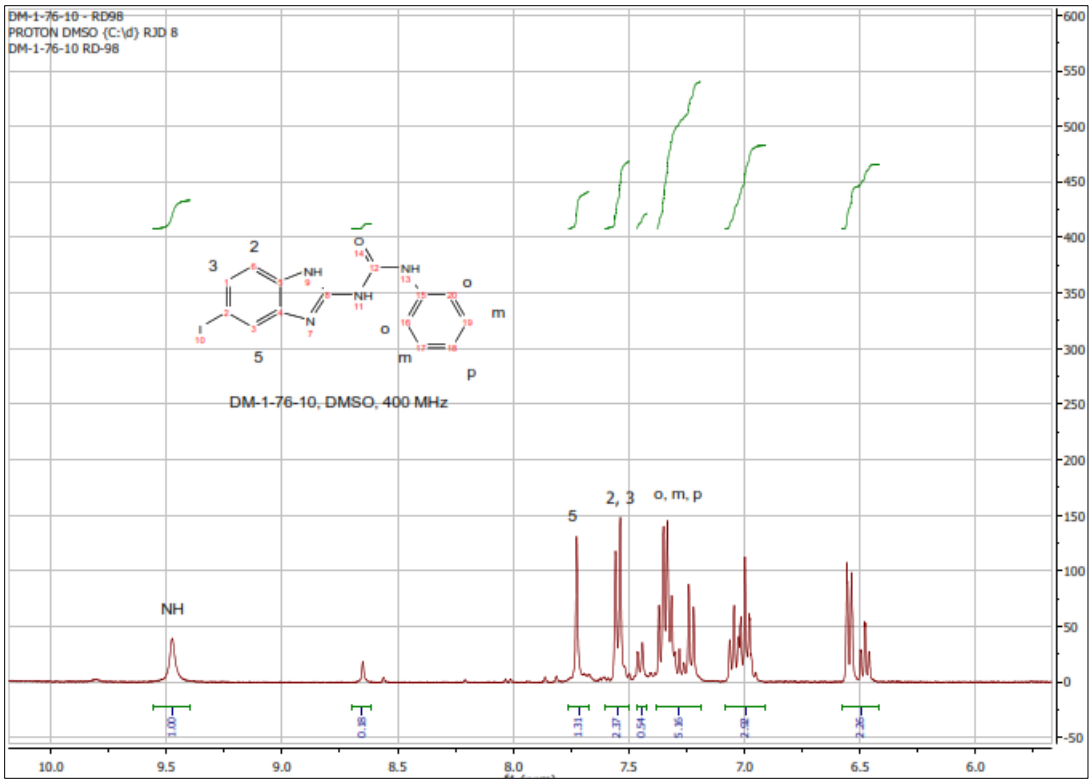

B

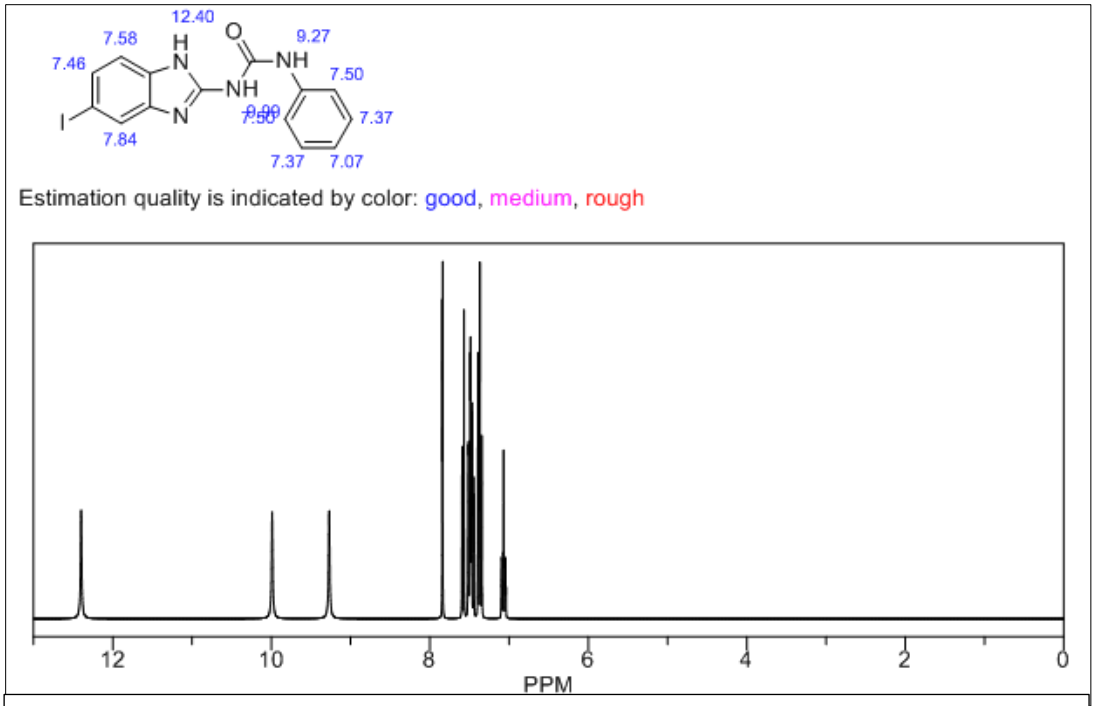

<u>Figure 25.</u> Proton NMR of 1-(6-Iodo-1H-benzo[d]imidazole-2-yl)-3-phenylurea in DMSO

A. Blowup of region of interest, solvent peaks not shown. Peaks assigned based on predicted chemical shifts (in DMSO via ChemDraw **B**)

Phase I *in vitro* Metabolism

Solutions

1) 898 µL Assay Buffer. **A** 100 mL stock solution was prepared (100 mM Trizma, pH=7.4, 3 mM $MgCl_2$) using 10 mL of Trizma (T2663-1L, 1.0 M) and 0.061 g $MgCl_2 \cdot 6H_2O$, which was empicarilly found to enhance the microsomal drug-metabolizing enzyme systems directly since it gave a better results suggesting that the microsomes are more active in presence of magnesium ion (Marvin, 1970). HCl (0.100 M) used to adjust pH.

2) 25 µL Microsomal Protein. 25 µL of 0.5 mg/mL microsomal protein (purchased as 20 mg/mL, or 10 mg/0.5 mL; MX008061, pooled male, 10 mg/$190 was used as is. BioreclamationIVT, 410-455-1242). The 10 mg/0.5 mL commercial material was divided into 20 plastic 1.5 mL microcentrifuge vials containing 25 µL each. Stored vials in -80°C freezer or in liquid nitrogen Dewar.

3) 2 µL Substrate Solution. 1 mL solution (25 µM) was made using 1.3 mg in 1.0 mL acetonitrile, methanol, or DMSO. Latter is preferred.

4) 75 µL NADPH. A fresh solution was made for each run. The 50 mg commercial sample (N1630-50mg, $115) was divided into 50 plastic 1.5 mL microcentrifuge vials containing 1.0 mg each. 100 µL of assay buffer was added to a vial for each run to obtain 1.0 mM. The total volume for each microsomal incubation tube was 1 mL.

Procedure

Incubations were performed in 16x100 mm glass culture tubes placed in a reciprocating water bath, set at 37°C. A microsomal protein vial (25 µL of 0.5 mg/mL) was allowed to warm to ice bath temperature and then the 898 µL of assay buffer (100 mM Tris, pH=7.4, 3 mM $MgCl_2$) was added. The mixture was added to the glass culture tube. 2 µL of substrate solution (25 mM compound) was added to the mixture, which was vortexed to mix and then pre-incubated for 5 minutes at 37°C. The reaction was initiated by the addition of 75µL of 1 mM NADPH solution (NADPH and assay buffer). Aliquots of 300 µL were removed from this incubation tube at 15, 30, and 60 minutes. A zero point control was set up by adding all of the above reagents except the microsomal protein (to account for the volume, 25 µL of assay buffer was added in its place). Two aliquots of 300 µL were removed from this control incubation, one as soon as components were mixed and another at 60 minutes.

500 µL of acetonitrile was added to each aliquot as soon as it was taken, vortexed, transferred to a microcentrifuge tube, and centrifuged at 16,000 rcf for 3 minutes. The supernatant was transferred to a clean LC/MS vile. Sample was injected into the LC/MS.

Compound Concentration Calculation

All samples were quantitatively analyzed by LC/MS on an Agilent 1100 series HPLC and recorded on a Waters TOF, Micromass-LCT using an Analytical Advantage ECHELON C18 column using the mobile phase gradient described in **Table 3.**

To determine the relative concentration of compounds using MS analysis, the molecular weight peak, or the major fragment ion if more intense than the molecular weight peak, was selected for in the MS TIC (total ion current) liquid chromatogram. Integration of the selected ion peak areas vs. time indicates the relative concentration of compound at the given time, from which metabolic rate was calculated.

Identification of Metabolites

To identify the metabolites for every RD compound synthesized and studied in the Doll Lab, the following procedure was utilized:

1. The raw MS TIC chromatogram does not provide useful information since the solution contains only traces of the parent compound and metabolites amongst, microsomal components, NADPH, and solvent. Thus, relevant information cannot be derived from it directly. An example of the original MS TIC is shown in **Figure 26a.**

2. To retrieve useful information from this MS TIC chromatogram, the parent peak is followed by searching for its corresponding molecular weight plus 1 (MW+1), as shown in **Figure 26b**, since molecules are ionized in the MS.

3. To identify the metabolites, peaks corresponding to the molecular weight plus a hydroxyl (MW+16) were extracted from the original chromatogram as depicted in **Figure 26c**. The ions comprising the TIC chromatogram peak can then be determined, allowing the assignment of structures to the ions (See **Figure 27**).

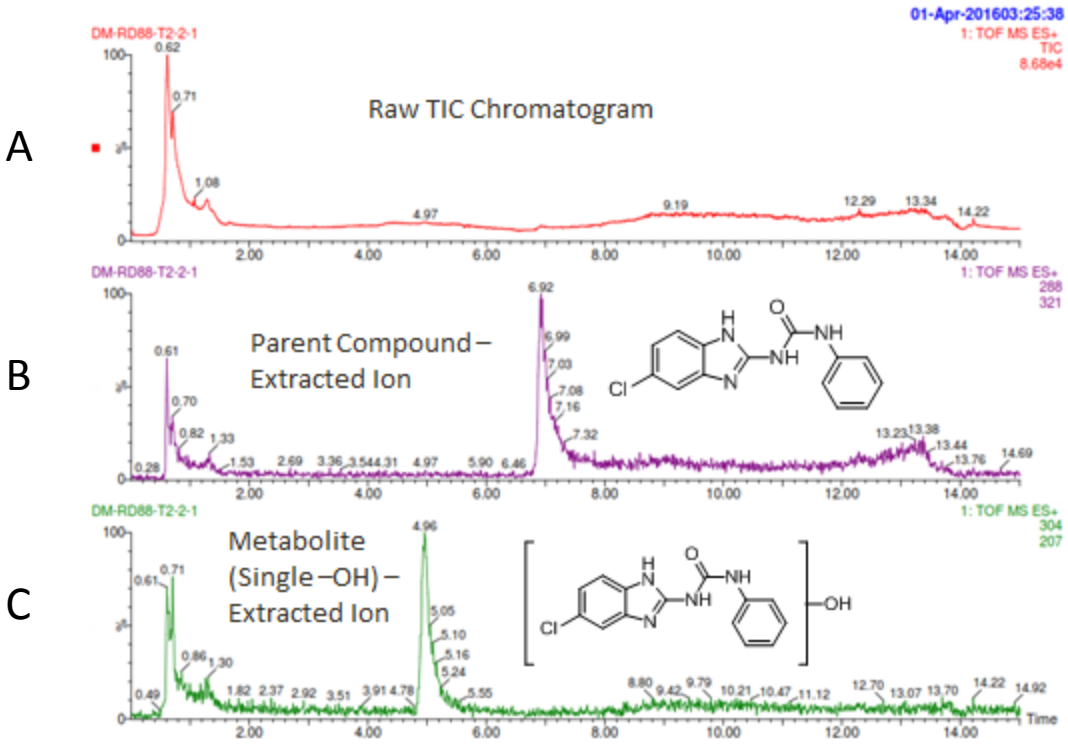

Figure 26. **Example of Ion extraction**
A. Raw MS TIC chromatogram. **B.** Extracted ion chromatogram for parent compound (M+1). **C.** Extracted ion chromatogram for single hydroxylation metabolite (M+16).

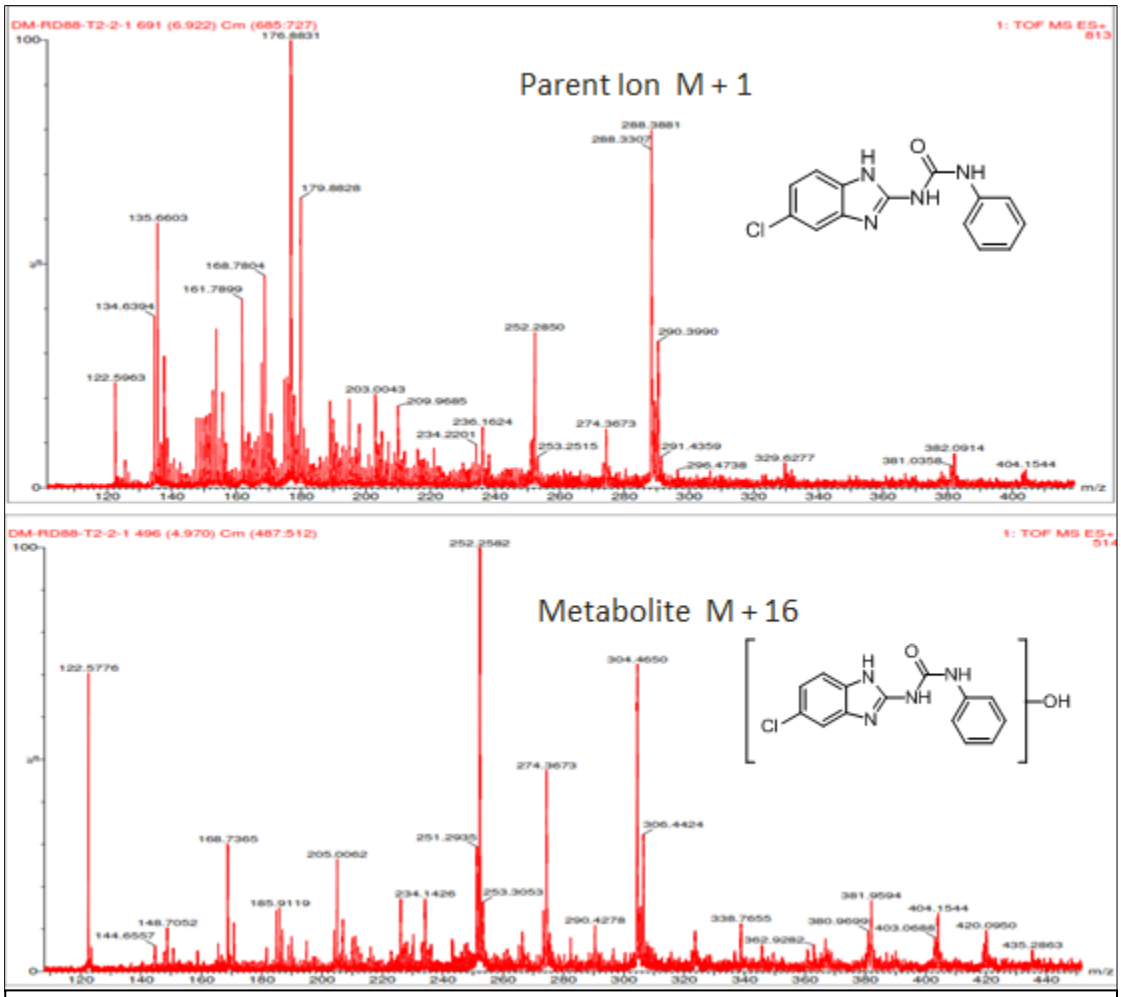

Figure 27. **Example of ions within M+1 TIC peak and M+16 TIC peak**
Top panel depicts ions present in parent compound chromatogram peak (M+1). Bottom panel depicts ions present in metabolite (M+16) chromatogram peak.

Metabolic Rate Calculations

All concentrations were obtained by the integration of the peak that was mass-selected (M+1) from the raw TIC chromatogram, converted to percent remaining of compound, and normalized to the natural log scale before being plotted in order to generate a first order rate of decay plot. Percentages were calculated based on the initial

concentration of compound, which was obtained from the zero time point control. A scatter plot of ln [% remaining compound] versus time, with a linear trend line, was computed using Microsoft® Excel. Half-life ($t_{1/2}$) calculations were done using the slope of the line (first order rate constant) in the following equation (2):

$$t_{1/2} = \frac{\ln(2)}{-slope \ln(\%remaingdrug)} \quad (2)$$

Since each experiment was performed in triplicates, error bars were obtained for each data point. The error bars utilized were obtained by the standard error, calculating the standard error of the mean corresponding to each data point. The standard error is calculated by dividing the standard deviation by the square root of number of measurements that make up the mean (often represented by N). In this case, 3 measurements were made (N = 3) so the standard deviation was divided by the square root of 3, as shown in equation (3). With the standard errors calculated for each concentration at each data point, Y error bars were introduced by entering the error amount, as the error bar method in Excel.

$$SE_{\bar{x}} = \frac{s}{\sqrt{n}} \quad (3)$$

Using the obtained value of $t_{1/2}$, the *in vitro* intrinsic clearance (Cl_{int}) was calculated according to equation (4).

$$Cl_{\text{int}} = \frac{\ln(2)}{t_{1/2}} * 0.5 \frac{mL_{incubation}}{mg_{microsomalprotein}} * 45 \frac{mg_{microsomalprotein}}{g_{liver}} * 21 \frac{g_{liver}}{kg} \quad (4)$$

Data was entered and analyzed using Microsoft® Excel, 2010 version. This procedure was followed for all analogs, except in the case of RD 98 (Iodo- analog) due to its rapid metabolism (see **Figures 30-32**).

RESULTS

The chloro-benzimidazole urea (RD 88) was the first final product to be synthesized, and the first to be subjected to the metabolism assay. However the first trial yielded data points with large standard error bars, thus the assay was repeated in a second trial which yielded quite different results (**Figure 28**). The data from the first trial indicated that RD 88 had a $t_{1/2}$ of 19.36 minutes, while the second trial indicated that RD 88 was metabolized at a much slower rate, as the data indicated the *in vitro* $t_{1/2}$ to be 68.63 minutes (**Table 5**). Additionally the standard error bars of these two trials overlap when plotted on the same graph.

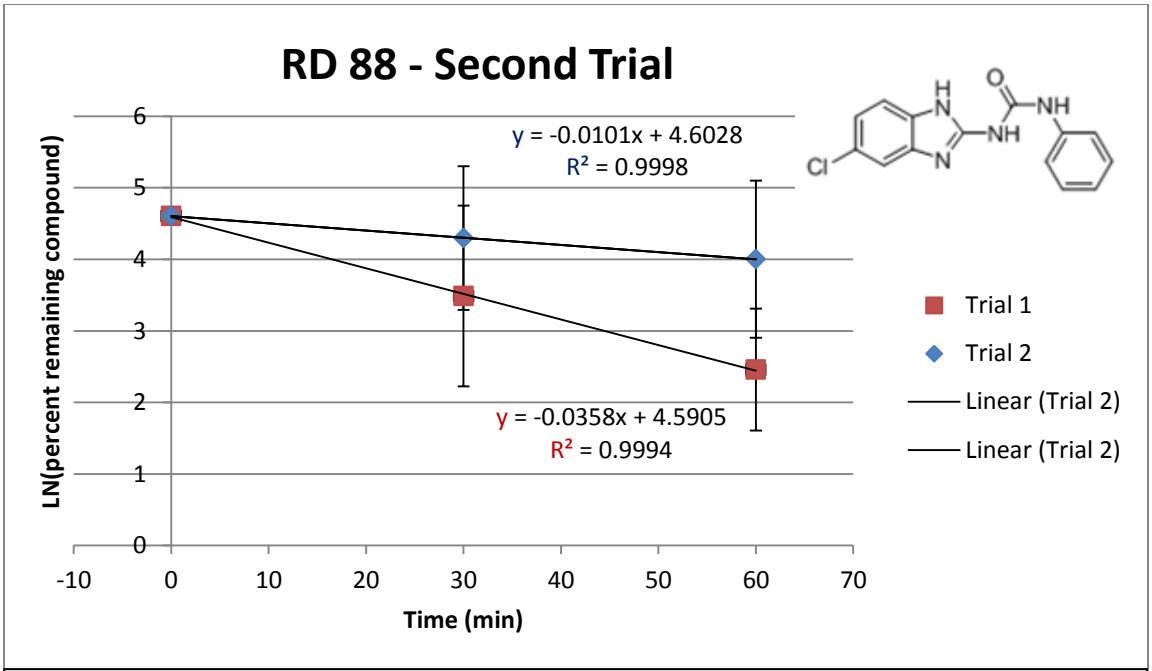

Figure 28. The disappearance of parent compound through metabolism by CYP450s
Relative concentrations taken from LC/MS data, converted to percent of remaining compound and normalized to natural log scale. Two separate trials of RD88 on metabolism assay yielded conflicting results.

Table 5. Half-life and intrinsic clearance of RD 88

	Trial 1	Trial 2
$T_{1/2}$	19.36 min	68.63 min
Cl_{intrs}	17.9 µL/min/mg protein	5.1 µL/min/mg protein

On the other hand, a single trial of the bromo-benzimidazole urea (RD 97) yielded data with small standard error bars (**Figure 29**), and a $t_{1/2}$ of 25.2 minutes, which was also comparable to half-lives of similar compounds determined by S. Sanchez's work (**Table 6**).

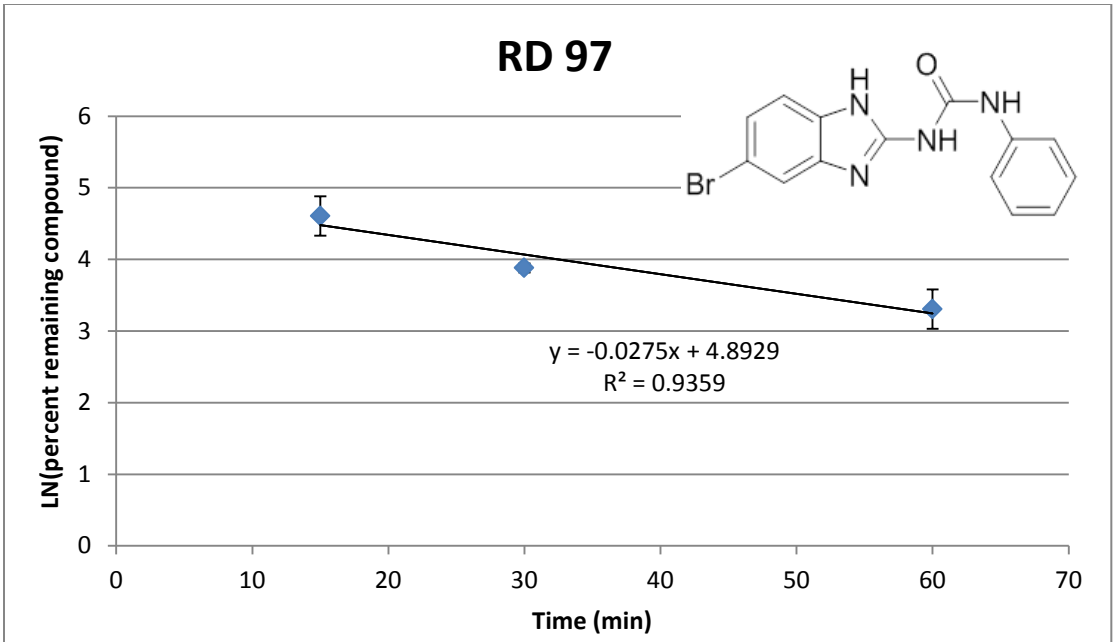

Figure 29. The disappearance of parent compound through metabolism by CYP450s
Relative concentrations taken from LC/MS data, converted to percent of remaining compound and normalized to log scale.

Table 6. Half-life and intrinsic clearance of RD 97

$T_{1/2}$	25.2 min
Cl_{intrs}	13.8 µL/min/mg protein

Lastly, the results of the trial of the iodo-benizmidazole urea (RD 98) in the metabolism assay were quite different that RD 88 & RD 97. In the crude data analysis, the parent ion of RD 98 was not able to be detected in any of the samples after the T_0 time point. To confirm this finding RD 98 was run in tandem with RD 88 (at the same time and under the same conditions). LC/MS analysis of this run indicated that the parent ion of RD 98 was present at T_0 but not at T_1 (or any later time points) (**Figure 30**), while

the parent ion was detectable at T_0 as well as T1 (**Figure 31**). It was believed that the early disappearance of the parent ion was due to rapid metabolism of the parent compound, thus indicating that RD 98 was uniquely metabolized at a much faster rate.

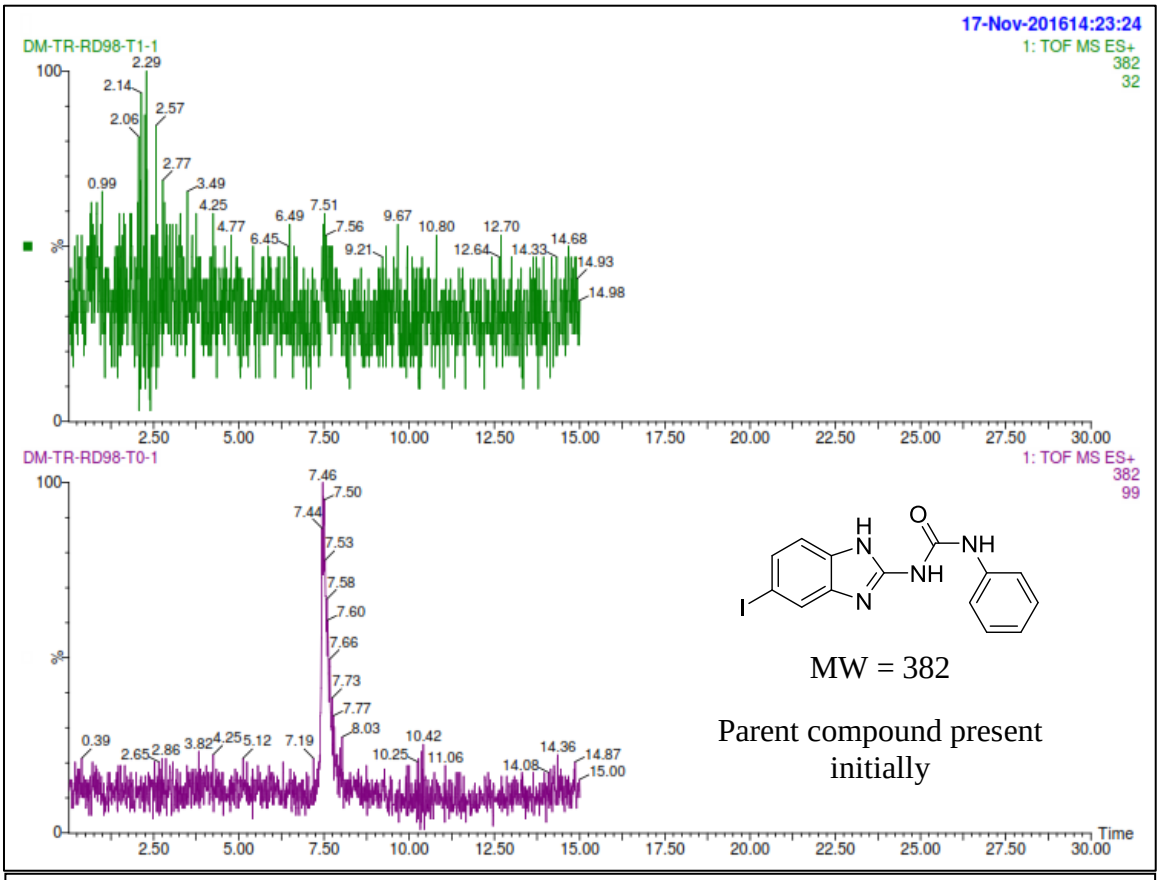

Figure 30. Ion-extracted Chromatogram of RD 98 metabolism run at T_0 and T_1
Ion extracted from raw TIC chromatograms. Parent compound no longer detected by LC/MS at 15min (T_1).

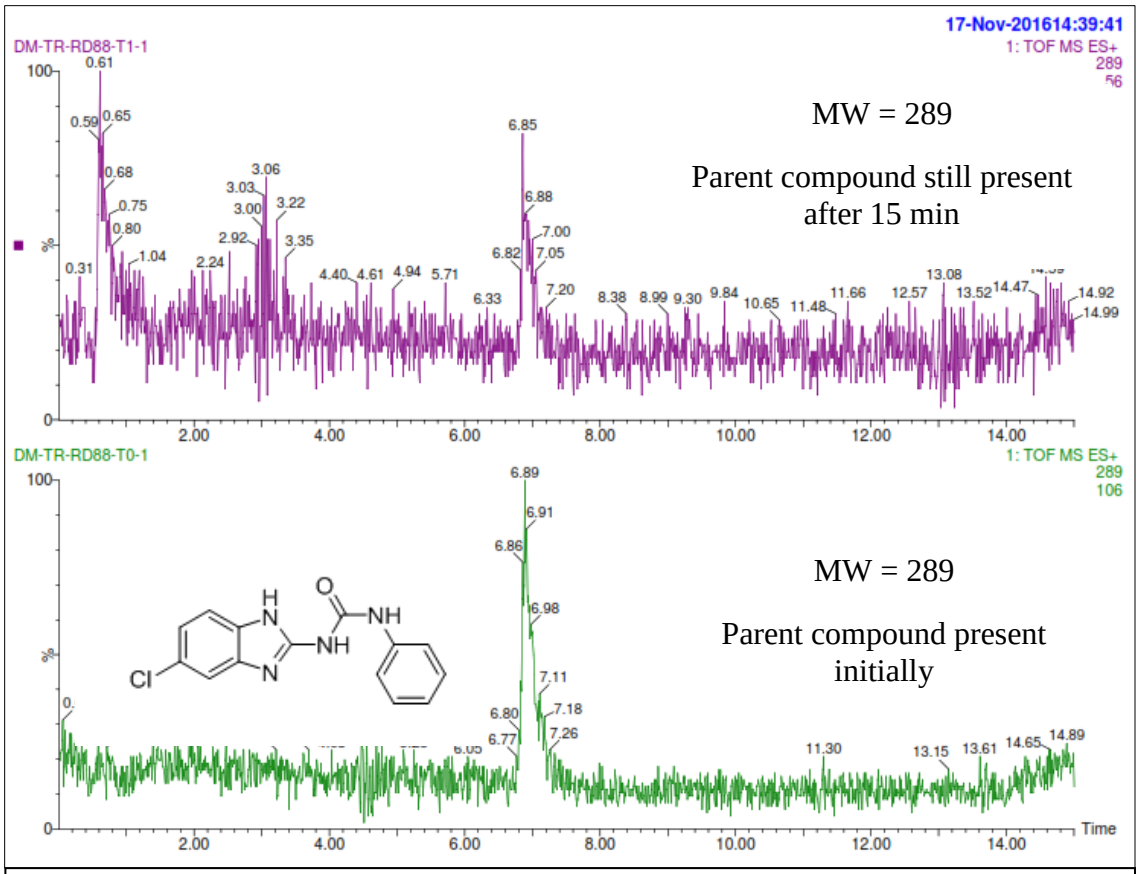

Figure 31. Ion-extracted Chromatogram of RD 88 metabolism run at T_0 and T_1
RD 88 was run in tandem with RD 98 (at the same time, under same conditions), with parent ion detected at both T_0 and T_1.

To confirm that the disappearance of the parent ion of RD 98 was due to metabolism, attempts were made to determine if metabolites of RD 98 could be found in the samples. An M+16 ion (single hydroxylation metabolite) was detected in both the T_2 and T_3 time points (30 and 60 minutes respectively), which had a lower retention time than the parent ion (as expected to result from increased polarity due to the added hydroxyl) (**Figure 32**). This evidence confirms that the disappearance of RD 98 in our assay is due to its rapid metabolism.

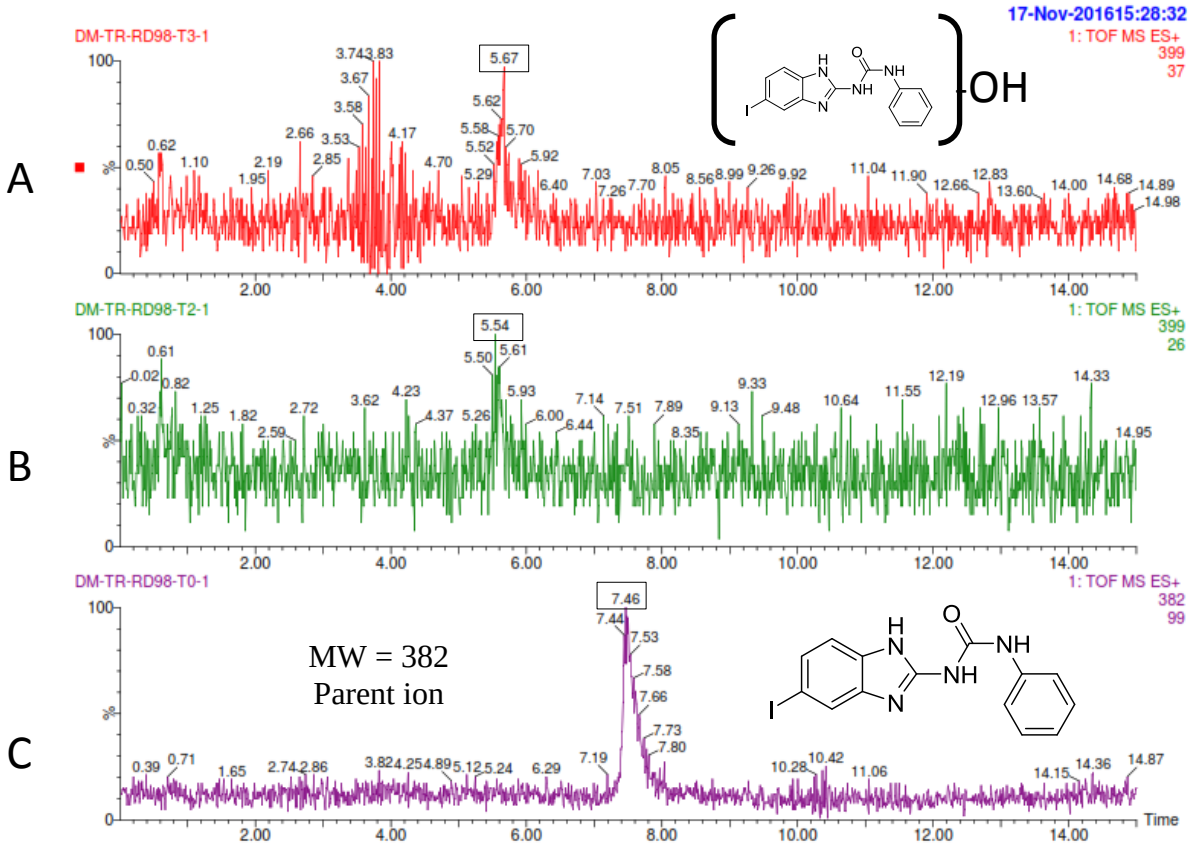

Figure 32. Ion-extracted Chromatogram of RD 98 parent ion and metabolite **A.** Presence of single hydroxyl-metabolite (M +16) at T_3 (60min) (at an earlier retention time that parent ion (**C**) as expected due to increase in polarity from added hydroxyl). **B.** Presence of single hydroxyl-metabolite (M +16) at T_2 (30min). **C.** Parent ion (M+1) peak (only present at T_0) with a clearly different retention time than proposed metabolite.

A summary table of results was compiled for the compounds synthesized in this study, along with similar compounds (benzimidazole-ureas) synthesized for a previous study (Sánchez 2016) (see **Table 7**).

Table 7. Summary Results

Compound	Half-life (t1/2) (min)	In Vitro Intrinsic Clearance (Clint) (µL/min mg protein)	Metabolite(s)
* H (RD 38)	15 ± 2.42	23.1	Single hydroxylation
* F (RD 83)	30 ± 2.06	11.5	Single hydroxylation
Cl (RD 88)	19.3	17.9	Single hydroxylation
	68.6	5.05	
Br (RD 97)	25.2	13.8	Single hydroxylation
I (RD 98)	<< 15	CBD	Single hydroxylation

*Results of work of S. Sánchez (Sánchez 2016).

DISSCUSSION

Characterization Data

Synthesis of 4-Chloro-2-aminobenzimidazole (Chloro- Intermediate) was successful indicated by 100% purity of LC/MS (**Figure 11**) with a parent peak at the proper molecular weight (167.9 m/z) (**Figure 12**). This allowed for the successful synthesis of 1-(6-Chloro-1H-benzo[d]imidazole-2-yl)-3-phenylurea (RD 88) indicated by 100% purity of LC/MS (**Figure 17**) with a parent peak at the proper molecular weight (287.2 m/z) (**Figure 18**). And H^1NMR peak assignments (**Figure 19a**) were comparable to the estimations provided by ChemDraw (**Figure 19b**).

Synthesis of 4-Bromo-2-aminobenzimidazole (Bromo- Intermediate) was successful indicated by 100% purity of LC/MS (**Figure 13**) with a parent peak at the proper molecular weight (211.7 m/z) (**Figure 14**). This allowed for the successful synthesis of 1-(6-Bromo-1H-benzo[d]imidazole-2-yl)-3-phenylurea (RD 97) indicated by 100% purity of LC/MS (**Figure 20**) with a parent peak at the proper molecular weight (332.4 m/z) (**Figure 21**). And H^1NMR peak assignments (**Figure 22a**) were comparable to the estimations provided by ChemDraw (**Figure 22b**).

Synthesis of 4-Iodo-2-aminobenzimidazole (Iodo- Intermediate) was successful indicated by ~85% purity of LC/MS (**Figure 15**) with a parent peak at the proper molecular weight (261.0 m/z) (**Figure 16**). This material was used to successfully synthesize 1-(6-Iodo-1H-benzo[d]imidazole-2-yl)-3-phenylurea (RD 98) indicated by 100% purity of LC/MS (**Figure 23**) with a parent peak at the proper molecular weight

(379.3 m/z) (**Figure 24**). And H^1NMR peak assignments (**Figure 25a**) were comparable to the estimations provided by ChemDraw (**Figure 25b**).

Metabolism Assays

RD 88

When the chloro-compound (RD 88) was initially tested through the metabolism assay, the data indicated that the compound had a $T_{1/2}$ of 19.36 min and a Cl_{intrs} of 17.9 µL/min/mg protein (**Table 5**) and these values were comparable to results that were previously seen for similar compounds (**Table 7**). However standard error bars indicated that there was a rather large margin of error for several data points in this trial (**Figure 28**) and thus a second trial was performed using chloro-compound. Surprisingly the second trial yielded a vastly different result ($T_{1/2}$ = 68.63 min, Cl_{intrs} = 5.1 µL/min/mg protein) that also displayed a large margin of error for several data points (**Figure 28**). This second result would suggest that metabolism of RD 88 occurred at a slower rate than initially indicated by the first trial. Furthermore, the second trial indicated addition of a chlorine atom inhibited metabolism to a remarkable degree ($T_{1/2}$ went from 15 min to 68.63 min) even more so than the addition of a fluorine atom (RD 83) ($T_{1/2}$ increased from 15 min. to 30 min) (**Table 7**). These conflicting results could be due to pipetting errors when aliquots are taken or inconsistency in the timing of the reaction quench (addition of acetonitrile inactivate enzymes). Nevertheless the assay needs to be repeated using RD 88 until consistent data is achieved (with a relatively low degree of error)

before conclusions can be drawn about RD 88 and how the chlorine atom affects the rate of metabolism for our compounds.

RD 97

Conversely, when the bromo-compound (RD 97) was initially tested through the metabolism assay the produced data indicated that the compound had a $T_{1/2}$ of 25.2 min and a Cl_{intrs} of 13.8 µL/min/mg protein (**Table 6**) and there was a relatively low degree of standard error between triplicates, indicated by small standard error bars (**Figure 29**). These data indicated that addition of the bromine atom was able to inhibit the metabolism of the compound compared to the unsubstituted analog (RD 38) ($T_{1/2}$ increased from 15 min to 25.2 min upon addition of bromine atom) however it was not able to inhibit metabolism to the same degree as the fluorine atom (which increased $T_{1/2}$ to 30 min) (**Table 7**). Although standard error appeared to be low, this assay should be repeated using with all compounds in order to ensure that these results are accurate representations of the PK of these compounds.

RD 98

When metabolism analysis was attempted for the iodo- compound (RD 98) parent compound (molecular ion of ~332 m/z) was unable to be detected in all samples except time point zero (T_0) (**Figure 30**). This unique finding suggested that RD 98 (parent compound) completely disappeared somewhere between T_0 and 15 min, presumably due to its rapid and complete metabolism. In order to investigate this hypothesis (and to ensure that this finding was not due to a newly manifested error in the assay) RD 98 was

run in tandem with RD 88 (both compounds were subjected to the metabolism assay at the same time and therefore under the same conditions). This experiment confirmed that there was no detectable amount of RD 98 parent ion in any sample other than T_0 (**Figure 30**) and RD 88 parent ion was indeed still detected after 15 minutes (**Figure 31**). This experiment confirmed that the integrity of the assay was maintained and that rapid disappearance of parent ion was solely demonstrated by RD 98 in the metabolism assay. To further investigate whether this rapid disappearance of parent compound was due to its (complete) metabolism, attempts were made in order to find and determine probable metabolites (of RD 98). In the T_2 sample (time = 30 min) a single-hydroxyl metabolite was found indicated by the presence of a peak with a molecular weight of the parent compound + 16 (molecular weight of hydroxyl) (ion at ~399 m/z) (**Figure 31b**). In addition to being the correct molecular weight, the retention time (RT) of this metabolite was slightly faster (5.54 min) than that of the parent compound (7.46 min) as expected due to increase in polarity from the addition of the hydroxyl (**Figure 31b-c**). In the T_3 sample (time = 60) this same metabolite was detected (ion at ~399 m/z with a RT of ~5.5 min) along with what appeared to be a peak at RT~3.5 (with the same mass to charge ratio, 399 m/z) (**Figure 31a**). This second peak could indicate that another single-hydroxyl metabolite (since they have the same m/z) is present within the sample, but with the hydroxyl at a different position (indicated by the metabolites having different RTs, because a change in hydroxyl position could result in a change in polarity of the compound). This evidence appears to indicate metabolism of RD 98 is taking place

within the assay however it is uncertain if the apparent disappearance of the parent compound is strictly due to its metabolism.

As discussed earlier, compound-protein binding is possibility in the microsomes-based metabolism assay. Additionally, compounds that appear to bind more frequently to microsomal proteins are described as largely lipophilic molecules (McLure *et al.* 2000), and due to the iodine atom in RD 98 it is most lipophilic compound being evaluated in this study (ClogP = 4.63, highest of all of the analogs). This suggests that RD 98 might bind more readily to microsomal protein than the other compounds, which could explain how it is uniquely undetectable in the assay (except for at T_0). To further support this hypothesis, the T_0 sample was taken from the negative control (no microsomal protein added) and that could explain why RD 98 is detectable at T_0. A way of investigating this hypothesis would be to take T_0 from an actual sample (or perform negative control with microsomal protein and without NADPH – since metabolism should not occur in its absence) and see if RD 98 parent ion is detectable in this sample. If it is not detectable in T_0 under these conditions this would support the hypothesis that RD 98 is binding to microsomal protein and thus its metabolism is inhibited.

Another possible explanation for the unique result demonstrated by RD 98 could be that it is being metabolized by a different CYP450 isozyme than the other analogs. As discussed earlier, lipophilicity has been implicated as factor in CYP450 isozyme specificity (Lewis *et al.* 2004). Since RD 98 is the most lipophilic analog, it is conceivable that its lipophilicity exceeds the threshold of one isozyme (the isozyme that

is responsible for metabolizing the other analogs), and therefore is being metabolized by a different isozyme that it can bind to favorably (despite or due to its lipophilicity). This change in the isozyme that is conducting metabolism could explain why RD 98 is metabolized at a much faster rate than the other analogs.

Conclusions

The goal of this study was to determine how structural modifications, made to our p53 reactivating compounds, affected their *in vitro* human metabolic rate in order to optimize potency, selectivity and drug like properties (metabolic stability and membrane permeability). Confirming that compounds have suitable drug-like properties early on in drug development is crucial. This method prevents investing time and resources on the optimization of drugs with great activity but poor PK properties (such as metabolism, bioavailability, and membrane permeability), which will ultimately lead to an unsuccessful drug when introduced into clinical trials (Huang *et al.* 2010, Ljungman 2000). The two common PK measures of metabolic rate for drug discovery compounds are intrinsic clearance (Cl_{intrs}) and half-life ($t_{1/2}$). Clearance indicates how rapidly a drug is excreted from the body's circulatory system, while half-life measures the amount of time it takes for the compound to reach half its initial concentration in the circulatory system (Kearns and Di 2011). These measures allow for an estimation of proper dosing for the given drug, however *in vitro* and *in vivo* values for these parameters differ, due to many factors and biological barriers in the body, and thus, algorithms have been devised in order better compare these values (Kearns and Di 2011). Literature has shown that

human liver microsomes can be utilized in order to determine *in vitro* intrinsic clearance and half-life for various compounds using LC/MS analysis (Chiba *et al.* 2009, Lu *et al.* 2006, Lukman *et al.* 2013, Kearns and Di 2011). This methodology was followed to acquire metabolic data for 1-(6-Chloro-1H-benzo[d]imidazole-2-yl)-3-phenylurea, 1-(6-Bromo-1H-benzo[d]imidazole-2-yl)-3-phenylurea, and 1-(6-Iodo-1H-benzo[d]imidazole-2-yl)-3-phenylurea (RDs 88, 97, & 98 respectively) and their data were compared to that of the fluorinated and unsubstituted analogs.

The acceptable human *in vitro* half-life range for marketable drugs is approximately 20-50 minutes (Kearns and Di 2011). The half-life of the unsubstituted benzimidazole urea (RD 38), 15±2.42 min, did not fall within this range however the fluorinated analog (RD 86) indicated a half-life within this range (30±2.06 min). When subjected to the same assay and analysis, RD 88 (chloro-analog) produced inconsistent runs between trials (**Table 5**) and thus conclusions regarding the addition of chlorine and its affected on metabolism could not be ascertained. The inconsistency observed for RD 88 could be caused by several factors such as errors in enzyme or solution preparation which could lead to altered rates of the metabolism reaction. RD 97 (bromo- analog) was found to have an *in vitro* half-life of 25.2 min. This indicates that the bromine atom inhibited metabolism, however not as effectively as the fluorine atom (displayed larger $T_{1/2}$ of 30 min). Finally RD 98 (Iodo- analog) was subjected to the assay and analysis, however parent compound was undetectable sometime before the T_1 time point was taken (15 minutes). A possible explanation for this unique finding could be that RD 98 is metabolized by a different enzyme than the other analogs, resulting in a much different

rate of metabolism. However an alternative explanation for this finding is that RD 98 integrates into the microsomal membrane more readily than the other analogs (due to its greater lipophilicity) which results in the compound being unable to interact with the CYP450 enzymes thus inhibiting its metabolism.

While fluorine is very electronegative it also has a very small atomic radius, chlorine, bromine, and iodine have lower electronegativites but slightly larger atomic radii, with iodine being the largest, followed by bromine (**Figure 29**).

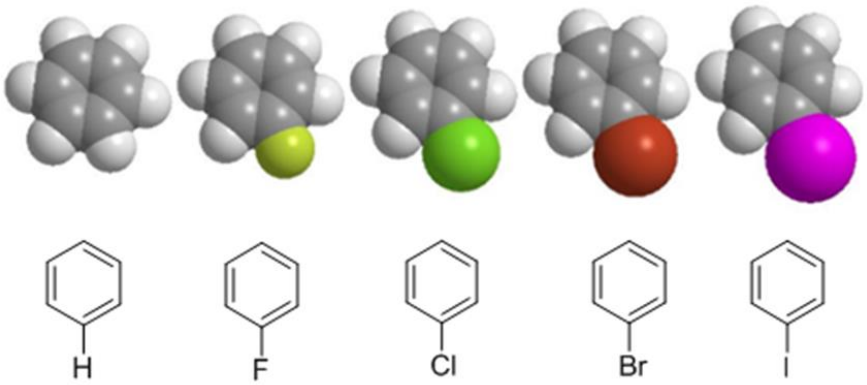

Atomic Radii (pm)	53	71	99	114	133
Electronegativity	2.1	4.0	3.0	2.8	2.5

Figure 33. Depiction of substituent size and electronegativity trends
Space filling model visually depicts size of atoms, while values are provided for atomic radii (pm) and electronegativity, for hydrogen and group 7 halogens.

It is clear that electronegativity of the substituent affects metabolism of the compound, however to our knowledge, the effect of steric hindrance on human metabolism by CYP450 enzymes has not been previously explored. However from these

comparison (fluorinated versus chlorinated versus brominated) we cannot determine with certainty if the size of the substituent will affect the metabolic rate of the compound or if this effect will be greater or lesser than that of electronegativity. Based on the current data it appears that electronegativity is the key factor that affects the metabolic activity of a compound. The fluorinated compound (RD 83) was the most effective at inhibiting metabolism, with the brominated compound (RD 97) inhibiting metabolism (compared to the unsubstituted compound) to a lesser degree as expected due to the lower electronegativity of bromine versus flourine (**Figure 30**). If the iodo-compound (RD 98) showed a half-life that was similar to or slightly larger than that of RD 97, we could conclude that size of substituent also effects metabolic rate, and it is not due to electronegativity alone. However the iodo-compound showed a remarkably different result, likely due to a different chemical property. Since RD 98 is more lipophilic than the other compound it is likely that the unique result of this compound is either due to microsomal protein binding or that a different CYP450 isozyme is responsible for its metabolism.

Future Considerations

In terms of future direction, replication of these assays for all analogs would be required in order to confirm with certainty their metabolic activity before drawing final conclusions. Additionally all compounds should be tested using the same microsomal protein batch as this would allow for a better comparison between metabolic stabilities of

the halogenated compounds. This is critical since enzymatic composition and activity can vary depending on the batch of microsomal protein.

Another parameter that should be investigated is the degree of microsomal protein binding to compound in our assay and how this varies depending on the compound structure. Microsomal protein binding may not pose a large issue if it effects all compounds equally (systematic error), however if degree is binding is influenced by the physiochemical properties of a compound (as expected) than this could lead to inaccurate representations and comparisons of the metabolic stability of our compounds. And the unique result produced by the iodo-compound could be an example of this.

Finally, determining which CYP450 isozyme metabolizes a drug can be done using CYP450 isozyme inhibitors, and this allows researchers to predict and prevent possible drug-drug interactions in the body (Kearns and Di 2011). Down the road, use of these inhibitors would prove beneficial in order to determine which isozyme metabolizes our compounds. This could be particularly helpful in elucidating the mechanism responsible for unique result of RD 98, since this result could be due to the compound being metabolism by another isozyme (than the other analogs). Ultimately this information would significantly improve the quality of the drug-like property profiles of our compounds, specifically in terms of metabolism, in order to help achieve our goal of accruing a sizeable library of potential p53 reactivating compounds with complete drug-like property profiles.

REFERENCES

Blackwell H, Frei R, Breitbach A, Lynn DM, Broderick AH, inventors. 2013. Inhibition and dispersion of bacterial biofilms with 2-aminobensimidazole derivatives. United States.

Bullock AN, Fersht A. 2001. Rescuing the function of mutant p53. Nature Reviews Cancer. 1(1):68-76.

CDC (Center for Disease Control & Prevention), U.S. Department of Health & Human Services. [Updated: 30 March 2017] Cancer Prevention and Control [Internet]. HSS/open website. [accessed in 2017 Jan 10.] Available from: http://www.cdc.gov/cancer/index.html

Chiba M, Ishii Y, Sugiyama Y. 2009. Prediction of hepatic clearance in human from in vitro data for successful drug development. Aaps Journal. 11(2):262-276.

Cui B, Yang Q, Guan HX, Shi BY, Hou P, Ji MJ. 2014. Prima-1, a mutant p53 reactivator, restores the sensitivity of tp53 mutant-type thyroid cancer cells to the histone methylation inhibitor 3-deazaneplanocin a. Journal of Clinical Endocrinology & Metabolism. 99(6):E962-E970.

Dasmahapatra B, Demma M, inventors; Zaradic S, agent. 2007 Nov 22. Development of a novel assay for MGMT (Methyl Guanine Transferase). United States patent PCT/US2007/010998.

Demma M, Maxwell E, Ramos R, Liang LZ, Li C, Hesk D, Rossman R, Mallams A, Doll R, Liu M et al. 2010. Sch529074, a small molecule activator of mutant p53, which binds p53 dna binding domain (dbd), restores growth-suppressive function to mutant p53 and interrupts hdm2-mediated ubiquitination of wild type p53. Journal of Biological Chemistry. 285(14):10198-10212.

Dorokhov YL, Shindyapina AV, Sheshukova EV, Komarova TV. 2015. Metabolic methanol: Molecular pathways and physiological roles. Physiological Reviews. 95(2):603-644.

Fasinu PS, Tekwani BL, Avula B, Chaurasiya ND, Nanayakkara NPD, Wang YH, Khan IA, Walker LA. 2016. Pathway-specific inhibition of primaquine metabolism by chloroquine/quinine. Malaria Journal. 15:12.

Freed-Pastor WA, Prives C. 2012. Mutant p53: One name, many proteins. Genes & Development. 26(12):1268-1286.

Foster BA, Coffey HA, Morin MJ, Rastinejad F. 1999. Pharmacological rescue of mutant p53 conformation and function. Science. 286(5449):2507-2510.

Giorgi C, Bonora M, Missiroli S, Morganti C, Morciano G, Wieckowski MR, Pinton P. 2016. Alterations in mitochondrial and endoplasmic reticulum signaling by p53 mutants. Frontiers in Oncology. 6:7.

Guengerich FP. 2008. Cytochrome p450 and chemical toxicology. Chemical Research in Toxicology. 21(1):70-83.

Hayashibara M. 2009. Interactions between grapefruit juice and calcium channel antagonists. Yonago Acta Medica. 52(1):1-9.

Huang LY, Berry L, Ganga S, Janosky B, Chen A, Roberts J, Colletti AE, Lin MHJ.

2010. Relationship between passive permeability, efflux, and predictability of clearance from in vitro metabolic intrinsic clearance. Drug Metabolism and Disposition. 38(2):223-231.

Joerger AC, Allen MD, Fersht AR. 2004. Crystal structure of a superstable mutant of human p53 core domain - insights into the mechanism of rescuing oncogenic mutations. Journal of Biological Chemistry. 279(2):1291-1296.

Kerns EH, Di L. 2008a. Drug-like properties: Concepts, structure design and methods: From adme to toxicity optimization. 30 Corporate Drive, Suite 400, Burlington, MA 01813, USA: Elsevier Academic Press. p. 1-526.

Kim S, An SSA. 2016. Role of p53 isoforms and aggregations in cancer. Medicine. 95(26):6.

Lambert JMR, Moshfegh A, Hainaut P, Wiman KG, Bykov VJN. 2010. Mutant p53 reactivation by prima-1(met) induces multiple signaling pathways converging on apoptosis. Oncogene. 29(9):1329-1338.

Lewis DFV, Jacobs MN, Dickins M. 2004. Compound lipophilicity for substrate binding to human p450s in drug metabolism. Drug Discovery Today. 9(12):530-537.

Liu JO, Shim JS, Chong CR, Bhat S, inventors; Corless PF, agent. 2010 Apr 15. Quinoline compounds as inhibitors of angiogenesis, human methionine aminopeptidase, and SIRT1, and methods of treating disorders. United States patent PCT/US2009/005475.

Ljungman M. 2000. Dial 9-1-1 for p53: Mechanisms of p53 activation by cellular stress. Neoplasia. 2(3):208-225.

Lu C, Li P, Gallegos R, Uttamsingh V, Xia CQ, Miwa GT, Balani SK, Gan LS. 2006. Comparison of intrinsic clearance in liver microsomes and hepatocytes from rats and humans: Evaluation of free fraction and uptake in hepatocytes. Drug Metabolism and Disposition. 34(9):1600-1605.

Lukman S, Lane DP, Verma CS. 2013. Mapping the structural and dynamical features of multiple p53 dna binding domains: Insights into loop 1 intrinsic dynamics. Plos One. 8(11):19.

Mantovani F, Walerych D, Del Sal G. 2016. Targeting mutant p53 in cancer: a long road to precision therapy. The Federation of European Biochemical Societies Journal. 1-14.

McLure JA, Miners JO, Birkett DJ. 2000. Nonspecific binding of drugs to human liver microsomes. British Journal of Clinical Pharmacology. 49(5):453-461.

Mizuno N, Niwa T, Yotsumoto Y, Sugiyama Y. 2003. Impact of drug transporter studies on drug discovery and development. Pharmacological Reviews. 55(3):425-461.

Nassar AEF, Kamel AM, Clarimont C. 2004. Improving the decision-making process in the structural modification of drug candidates: Enhancing metabolic stability. Drug Discovery Today. 9(23):1020-1028.

Nichols J, Erhardt S, Dyer S, James M, Moore M, Plotzke K, Segner H, Schultz I, Thomas K, Vasiluk L et al. 2007. Use of in vitro absorption, distribution, metabolism, and excretion (adme) data in bioaccumulation assessments for fish. Human and Ecological Risk Assessment. 13(6):1164-1191.

Ning J, Yu ZL, Hu LH, Wang C, Huo XK, Deng S, Hou J, Wu JJ, Ge GB, Ma XC et al.

2015. Characterization of phase i metabolism of resibufogenin and evaluation of the metabolic effects on its antitumor activity and toxicity. Drug Metabolism and Disposition. 43(3):299-308.

Obach RS. 1999. Prediction of human clearance of twenty-nine drugs from hepatic microsomal intrinsic clearance data: An examination of in vitro half-life approach and nonspecific binding to microsomes. Drug Metabolism and Disposition. 27(11):1350-1359.

Rosenblum SB, Huynh T, Afonso A, Davis HR, Yumibe N, Clader JW, Burnett DA. 1998. Discovery of 1-(4-fluorophenyl)-(3r)- 3-(4-fluorophenyl)-(3s)-hydroxypropyl -(4s)-(4- hydroxyphenyl)-2-azetidinone (sch 58235): A designed, potent, orally active inhibitor of cholesterol absorption. Journal of Medicinal Chemistry. 41(6):973-980.

Ruiz-Garcia A, Bermejo M, Moss A, Casabo VG. 2008. Pharmacokinetics in drug discovery. Journal of Pharmaceutical Sciences. 97(2):654-690.

Sanchez SC. 2016. Evaluation of Human Liver Metabolism of Compounds that Reactivate Mutant p53 in Human Cancer Cells [thesis]. Drew University-Madison. 88 p.

Seger ST, Rydberg P, Olsen L. 2015. Mechanism of the n-hydroxylation of primary and secondary amines by cytochrome p450. Chemical Research in Toxicology. 28(4):597-603.

Sousa MC, Braga RC, Cintra BAS, de Oliveira V, Andrade CH. 2013. In silico metabolism studies of dietary flavonoids by cyp1a2 and cyp2c9. Food Research International. 50(1):102-110.

Sridhar J, Liu JW, Foroozesh M, Stevens CLK. 2012. Insights on cytochrome p450 enzymes and inhibitors obtained through qsar studies. Molecules. 17(8):9283-9305.

Sun HM, Veith H, Xia MH, Austin CP, Huang RL. 2011. Predictive models for cytochrome p450 isozymes based on quantitative high throughput screening data. Journal of Chemical Information and Modeling. 51(10):2474-2481.

Urso L, Calabrese F, Favaretto A, Conte P, Pasello G. 2016. Critical review about mdm2 in cancer: Possible role in malignant mesothelioma and implications for treatment. Critical Reviews in Oncology/Hematology. 97:220-230.

Ventura A, Kirsch DG, McLaughlin ME, Tuveson DA, Grimm J, Lintault L, Newman J, Reczek EE, Weissleder R, Jacks T. 2007. Restoration of p53 function leads to tumour regression in vivo. Nature. 445(7128):661-665.

Vogelstein B, Kinzler KW. 2004. Cancer genes and the pathways they control. Nature Medicine. 10(8):789-799.

Wiman KG. 2010. Pharmacological reactivation of mutant p53: From protein structure to the cancer patient. Oncogene. 29(30):4245-4252.

Wuitschik G, Rogers-Evans M, Muller K, Fischer H, Wagner B, Schuler F, Polonchuk L, Carreira EM. 2006. Oxetanes as promising modules in drug discovery. Angewandte Chemie-International Edition. 45(46):7736-7739.